

**A weather-regime based
stochastic weather generator for
climate scenario development
across Massachusetts**

Technical Documentation

**Scott Steinschneider
Nasser Najibi**

**Biological and Environmental Engineering
Cornell University
Ithaca, NY**

April 5, 2022

1. Introduction

Climate change poses a major threat to the sustainability of water systems. To better understand this threat, planners require future climate scenarios that are used to test the robustness of their system to different components of climate change. However, how these scenarios can be generated in an internally consistent and computationally efficient manner for risk-based water system studies remains an open question.

General Circulation Models (or Global Climate Models; GCMs) are a valuable tool for describing how physical processes in the climate system drive predictability and variability in local weather. Projections from these numerical models over multi-decadal timescales (Taylor et al., 2012) provide internally consistent scenarios that can be used to examine the impacts of anthropogenic climate change on water systems (Brekke et al., 2009; Jiménez Cisneros et al., 2014). The climate mechanisms that lead to these impacts can generally be categorized as either thermodynamic or dynamic modes of climate change (Emori and Brown, 2005; Seager et al., 2010, 2014). Thermodynamic climate changes relate directly to the increased surface warming of the Earth under anthropogenic forcing. These changes include shifts in extreme heat, snow accumulation and melt, and the intensification of the water cycle (i.e., greater evapotranspiration and enhanced droughts (Dai, 2011; Trenberth et al., 2014) and more intense precipitation resulting from increases in the moisture carrying capacity of a warmer atmosphere (Trenberth, 2011). These types of thermodynamic climate changes are consistent across theory, observations, and model projections (IPCC 2013; Pfahl et al., 2017), leading to high confidence in the future direction of change, albeit with residual uncertainty in their magnitude.

Changes in atmospheric dynamics (i.e., the organization and persistence characteristics of atmospheric circulation) can also play a critical role in regional climate change (Lu et al., 2014; O’Gorman, 2015). However, these changes are significantly more uncertain than thermodynamic change (Shepherd, 2014; Pfahl et al., 2017), leading to large uncertainties in projected precipitation characteristics (Hawcroft et al., 2016; Shepherd, 2014; Woollings, 2010; Zappa et al., 2013; Stephens et al., 2010; Kysely et al., 2015; Tan et al., 2018). This complicates the direct use of GCM projections in long-term impact assessments. Improved GCM resolution does not necessarily improve precipitation biases linked to atmospheric dynamics (Muñoz et al., 2017; Maher et al., 2018), and when it does, there is necessarily a reduction in computational efficiency that limits ensemble simulations needed for risk-based assessments (Kendon et al., 2018). In addition, statistical corrections to these dynamical biases are far from straightforward, since they are linked to modeled physical processes that could change under global warming and thus change the bias over time (Stephenson et al., 2012; Maraun, et al. 2017).

Stochastic weather generators provide a computationally efficient and complementary alternative to GCMs for investigating water system performance under climate stress. These models are parameterized based on existing meteorological records and are then used to generate large ensembles of simulated daily weather records that are similar to but not bound by variability in past observations (Richardson, 1981; Wilks and Wilby, 1999; Fowler et al., 2007). For water system applications, weather generators must often develop sequences of multiple weather variables (e.g., precipitation, temperature) at multiple locations while maintaining realistic persistence and covariance structures associated with transient, multi-day storm events and over longer (seasonal-inter-annual) timescales. Once fit to historical data, model parameters can be

systematically altered to produce new traces of weather that exhibit a wide range of change in their distributional characteristics, including the intensity and frequency of average and extreme precipitation, heatwaves, and cold spells (Wilks, 2002, 2010, 2012).

This report documents work under a Phase I effort supported by the Massachusetts Executive Office of Energy and Environmental Affairs to utilize a stochastic weather generator to develop scenarios of climate change for the state of Massachusetts. The weather generator is designed to separately model thermodynamic and dynamic climate changes so that scenarios can be generated that isolate these different climate mechanisms and their potential impacts. The benefit of this approach is that scenarios can then be created that reflect more or less certain pathways of climate change, and end products can be tailored by decision makers to only reflect those pathways deemed sufficiently credible to be considered for planning purposes. This is in contrast to the direct use of downscaled GCM integrations, which unavoidably merge together mechanisms of dynamic and thermodynamic change and aspects of (uncorrectable) model bias into the final climate simulations. In this report, we develop, calibrate, and validate a stochastic weather generator across all HUC8 watersheds that intersect with the state of Massachusetts, and then develop a set of climate change scenarios for those watersheds that only reflect mechanisms of thermodynamic climate change deemed to be more credible. These thermodynamic climate changes are based on the range of temperature projections produced by a set of downscaled GCMs for the region. The results of the generated scenarios are then used to update projections made available to the public through the Resilient MA website (<https://resilientma.org/>). The generation of dynamic climate change scenarios with the stochastic weather generator is left for a latter phase of this work.

2. Data

2.1. Observational Data and Atmospheric Circulation based on Reanalysis

We collected observed daily precipitation [mm] and maximum and minimum temperature [C] time-series between January 1, 1950, and December 31, 2013 (64 years) from the gridded meteorological dataset for North America provided by Livneh et al. (2015) at a $0.0625^\circ \times 0.0625^\circ$ (~ 6-by-6 km) resolution. This gridded dataset applies the SYMAP algorithm to station data in the gridding process, in addition to an orographic scaling based on the PRISM algorithm (see more in Shepard (1984) and Daly et al. (1994)). These data were collected for 20 river basins (at 8-digit Hydrologic Unit Code: HUC8 level) that span the entire state of Massachusetts (Figure 1). These basins have drainage areas ranging from 1000 to almost 9000 km², and span a range of climatic conditions and precipitation regimes across the state. Gridded precipitation and temperature observations were extracted within and along the boundary for these basins. Table 1 provides detailed information about these basins, including dimensions of the compiled gridded data points.

We also obtained daily gridded ($2.5^\circ \times 2.5^\circ$) geopotential heights (GPH) [m] at the 500-hPa level from the National Centers for Environmental Prediction (NCEP)/National Center for Atmospheric Research (NCAR) reanalysis (NCEP/NCAR Reanalysis 1) dataset (Kalnay et al., 1996) between January 1, 1950, and December 31, 2017 (68 years). There are $t = 24,837$ days in this timespan. The gridded data were then extracted for the region between 30°N - 60°N and 110°W - 50°W , covering much of the Eastern half of the United States including the Northeast and western Atlantic basin.

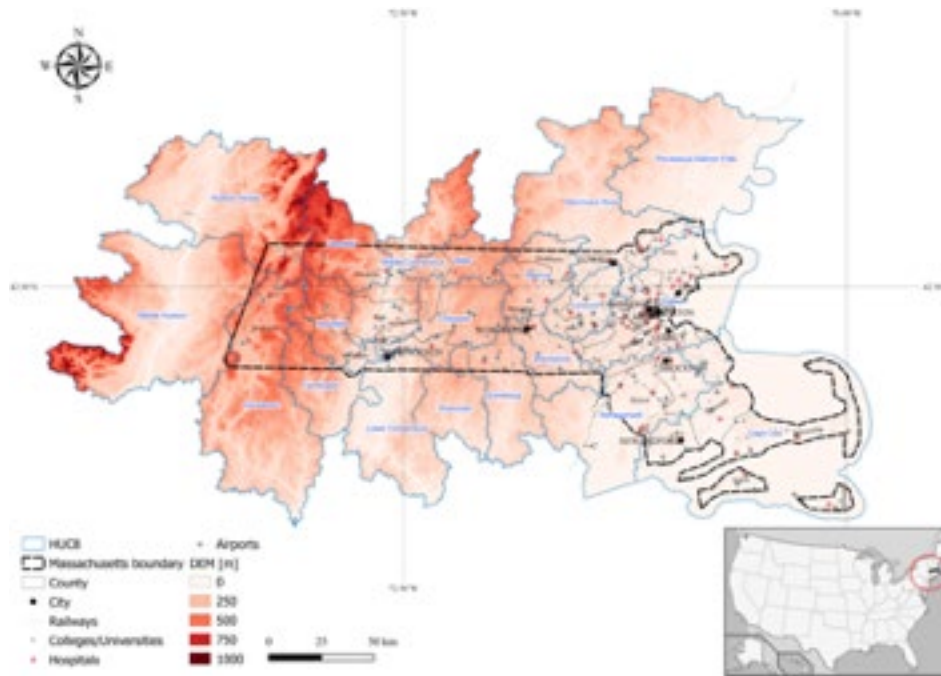


Figure 1. HUC8 watersheds across the state of Massachusetts that are modeled with the stochastic weather generator.

Table 1. Properties of HUC8 watersheds across Massachusetts.

Basin Number	Basin Name	HUC8	State	Area [km ²]	# Gridded Points
1	Piscataqua-Salmon Falls	01060003	MA,ME,NH	4475.36	118
2	Middle Hudson	02020006	MA,NY	6291.95	176
3	Narragansett	01090004	MA,RI	3843.17	103
4	Charles	01090001	MA	3867.51	93
5	Farmington	01080207	CT,MA	1571.6	44
6	Shetucket	01100002	CT,MA	1362.98	38
7	Lower Connecticut	01080205	CT,MA	2809.44	79
8	Westfield	01080206	CT,MA	1343.53	38
9	Quinebaug	01100001	CT,MA,RI	1913.53	55
10	Housatonic	01100005	CT,MA,NY	5053.66	140
11	Nashua	01070004	MA,NH	1379.21	39
12	Concord	01070005	MA	1036.63	30
13	Miller	01080202	MA,NH	1007.77	29
14	Chicopee	01080204	MA	1871.53	52
15	Cape Cod	01090002	MA,RI	8823.39	163
16	Merrimack River	01070006	MA,NH	4662.81	128
17	Middle Connecticut	01080201	MA,NH,VT	2636.71	72
18	Hudson-Hoosic	02020003	MA,NY,VT	4936.2	137
19	Blackstone	01090003	MA,RI	1228.46	33
20	Deerfield	01080203	MA,VT	1718.23	49

2.2. Downscaled Climate Model Projections

Scenarios of thermodynamic climate change developed using the stochastic weather generator are based on temperature projections from the Multivariate Adaptive Constructed Analogs (MACA) statistically downscaled product (Abatzoglou and Brown, 2012; Abatzoglou, 2013). MACA downscales global climate model (GCM) output from the CMIP5 ensemble to higher spatial resolutions while maintaining covariance patterns in multiple variables across space. These downscaled data are designed to ensure physical plausibility across a set of meteorological fields. The downscaling method includes bias correction via quantile mapping followed by a constructed analogs approach, in which a daily GCM synoptic field, or target pattern, is built by identifying and taking a linear combination of the 30 best predictor patterns from the observational record that are most similar to the GCM synoptic field. An epoch adjustment is employed that removes differences in the means between future and historical time periods to manage instances with no historical analogs under future climate scenarios.

Gridded MACA data are gathered for the period between 2006-2099 for grid cells across all HUC8 watersheds in and around the state of Massachusetts (see Figure 1). Monthly average minimum and maximum temperatures were gathered from these projections, and then were averaged to estimate average monthly mean temperature. Data were collected for the RCP 4.5 and 8.5 emission scenarios from 20 different climate models (see Table 2), although results in this report are only shown for RCP 8.5. We select the MACA product over other publicly available downscaled products for two reasons. First, the MACA product downscales a relatively large set of GCMs from the CMIP5 database, providing a better quantification of uncertainty compared to dynamically downscaled products based on a smaller set of GCMs (e.g., CORDEX, Jones et al. (2011)). Second, the MACA product was used for a separate analysis to scale intensity-duration-frequency (IDF) curves of extreme precipitation, and so to be consistent with that work, we retain the use of the MACA data in this study.

Table 2. Climate models used in this study. All projections were gathered for the RCP 4.5 and 8.5 scenarios.

GCMs			
(1) BCC-CSM-1-1	(6) CNRM-CM5	(11) HadGEM2-ES365	(16) MIROC5
(2) BCC-CSM-1-1m	(7) CSIRO-Mk3-6-0	(12) INMCM4	(17) MIROC-ESM
(3) BNU-ESM	(8) GFDL-ESM2G	(13) IPSL-CM5A-LR	(18) MIROC-ESM-CHEM
(4) CanESM2	(9) GFDL-ESM2M	(14) IPSL-CM5A-MR	(19) MRI-CGCM3
(5) CCSM4	(10) HadGEM2-CC365	(15) IPSL-CM5B-LR	(20) NorESM1-M

3. Methods

In the sections below, we first introduce the stochastic weather generator used throughout this report (Section 3.1). Then, we describe an approach to calibrate and validate the model across all HUC8 watersheds across Massachusetts (Section 3.2). Finally, we describe the scenarios of thermodynamic climate change developed using the model for each of the HUC8 watersheds (Section 3.3).

3.1. Stochastic Weather Generator

This report utilizes a semiparametric, multivariate, and multisite stochastic weather generator that was previously tested in the state of California and only for the cold season (Steinschneider et al.

2019; Najibi et al., 2021). This is the first application of the model to the Eastern United States and for the entire calendar year. The weather generator is designed to separately model dynamic and thermodynamic atmospheric mechanisms of climate variability and change through statistical abstractions of these processes. To capture atmospheric dynamics, the weather generator simulates sequences of weather regimes (WRs). WRs are recurring large-scale atmospheric flow patterns (e.g., upper-level, quasi-stationary blocks and troughs) that appear at fixed geographic locations, persist for days-to-weeks within a season, and organize high-frequency weather systems (Robertson and Ghil, 1999; Robertson et al., 2015). They represent intermediary phenomena in the stochastic continuum of atmospheric perturbations that connect local weather to hemispheric circulation, and provide a parsimonious way of abstracting major patterns of atmospheric circulation into stochastic simulations of weather. To capture thermodynamic mechanisms of climate change, the weather generator post-processes simulated data to reflect patterns of warming and thermodynamic scaling of precipitation rates with that warming. These properties of the model are represented in a hierarchical structure composed of three primary modules: 1) identification and simulation of WRs that dictate the large-scale atmospheric flow across the eastern US; 2) simulation of local weather in HUC8 watersheds conditioned on the WRs; and 3) perturbations to the simulation schemes in (1) and (2) reflective of thermodynamic climate change. These modules are described briefly below, and we point the reader to Steinschneider et al. (2019) and Najibi et al. (2021) for more detail.

3.1.1. Weather Regime Module

Following Najibi et al. (2021), we use Nonhomogeneous Hidden Markov Models (NHMMs) to identify WRs. NHMMs are nonlinear statistical models that use latent variables to identify clusters in state-space while simultaneously accounting for the distribution and temporal dynamics of observed data (Rabiner 1989, Hughes & Guttorp, 1994, Hughes et al., 1999). In this application, we first project 500-hPa geopotential height anomalies onto their first J empirical orthogonal functions (EOFs), where J is chosen using a scree test to ensure that the selected EOFs explain the majority (e.g., $> 90\%$) of the variance in the data. We then evaluate a first-order NHMM on the J PCs of geopotential heights to assign each day in the record to one of K separate WRs. The NHMM is fit using two harmonics as exogenous variables to account for seasonality in the WRs. Future time series simulations of WRs of an arbitrary length can be created through forward simulation of the fitted NHMM. Importantly, by using the NHMM, days are classified into WRs in a way that explicitly considers WR persistence, which will lead to persistent weather (i.e., longer dry and wet spells) in the weather generator simulations. The Expectation-Maximization algorithm (Dempster et al., 1977) is used to estimate the parameters of the NHMM. The expectation step is computed using the forward-backward algorithm (Baum and Petrie, 1966, Baum et al., 1970), and the expectation-maximization steps are iterated until convergence. The most probable sequence of hidden states is computed using the Viterbi algorithm (Forney 1973, Rabiner, 1989). In this work, we utilized the R-package ‘depmixS4’ (Visser and Speekenbrink 2010) to fit the NHMM.

3.1.2. Local Weather Generation Conditioned on Weather Regimes

Local weather for the HUC8 watershed of interest is simulated by bootstrapping weather data (e.g., daily precipitation, minimum and maximum temperature) based on sequences of simulated WRs. Assume that starting on simulation day t , the vector WR contains n days of the i^{th} WR (i.e., WR_t through WR_{t+n-1} equal i). Here, n usually varies from a single day to few weeks, although it can extend longer than 1 month due to the persistence of WRs. To generate weather for those n days,

we resample a n^* -day block of historical data that was also classified into the i^{th} WR, based on the absolute difference between the historical and simulated block length (i.e., a historical block with length n^* closer to n will receive a higher probability and will be resampled with a higher likelihood). We also require that any resampled blocks meet two other criteria: 1) the central day of the historical block is within a 20-day window of the day of year for simulation day t ; and 2) the day prior to the historical block has the same state of basin averaged precipitation (i.e., dry ($p_{avg} = 0 \text{ mm}$) or wet ($p_{avg} > 0 \text{ mm}$)). This ensures that the resampled data will preserve the seasonality of local weather and better maintains precipitation persistence across the basin.

If a historical block happens to be resampled with a longer length than the simulated one (i.e., $n^* > n$), we reduce the length of the resampled block by discarding days from that block (randomly from one of its two ends) until $n^* = n$. If the length $n^* < n$, then the remaining length $n - n^*$ is used as the basis to resample another block for WR i , and this process is continued until data has been resampled for the entire block of n days. At this point, the WR will change states and the resampling procedure begins again. By using this block bootstrap procedure, the resampled data are more likely to capture the entire life cycle of passing storms (and the resulting space-time structure in weather) over the basin of interest.

The block bootstrap will preserve many of the properties of the marginal and joint distributions of local weather variables, but at the expense of being able to simulate values outside the range of the instrumental record. To address this drawback specifically for precipitation, the weather generator uses a copula-based jittering approach. The copula-based jittering adds noise to the resampled precipitation data as a post-processing step. The noise is added to the non-exceedance probabilities of the resampled data across sites by month and WR assignment, and is then mapped back through Gamma distributions fit to each site by month and corresponding WR. This approach is designed such that final values of simulated, jittered precipitation can: 1) extend beyond the range of historical precipitation values; but preserve 2) the marginal distribution of precipitation at each site and 3) the rank correlation structure across sites. See Steinschneider et al. (2019) for more technical details about this block bootstrapping process.

3.1.3. Thermodynamic Climate Change Scenarios

We adopt an approach where climate perturbations are imposed specifically for thermodynamic processes, enabling a clearer link between local climate changes and their associated causal pathways. We argue that this strategy is well suited to facilitate the use of climate science to constrain and inform the likelihood of future climate changes and their impacts.

Temperature change is treated simply by adding trends to simulated temperature data for each location across the spatial domain. Currently, only step changes are permitted, but linear or quadratic trends are also possible. Using the weather generator, many (~ 10 's to 1000's) ensemble members of weather traces can be generated for any specified temperature scenario.

We use quantile mapping to scale the distribution of precipitation in a way that replicates the effects of warming temperatures on precipitation through increases in the moisture holding capacity of the atmosphere. Similar to other studies (Pendergrass and Hartmann, 2014a), we quantify precipitation-temperature scaling as a percent change in the moments and quantiles of the precipitation distribution per degree warming. Separate scaling rates are selected for the mean and

the 99.9th percentile of non-zero precipitation, by month and WR, and new parameters $\{\alpha_{CC}, \beta_{CC}\}$ of a Gamma distribution are determined by optimizing multiplicative perturbations $\delta_\alpha, \delta_\beta$ to the original shape and rate parameters ($\alpha_{CC} = \alpha \times \delta_\alpha$; $\beta_{CC} = \beta \times \delta_\beta$) to impose the selected scaling rates. Once the new Gamma parameters are determined for each site, month, and WR, daily simulated precipitation is adjusted by first determining the non-exceedance probability, then perturbing the non-exceedance probability using the copula-based jitter model (Section 3.1.2), and finally determining a new precipitation value based on the scaled Gamma distribution. This procedure is repeated for each nonzero precipitation amount for each site synthesized by the weather generator.

Importantly, the degree to which precipitation is scaled is directly tied to the temperature trends imposed, thus respecting the underlying thermodynamic mechanism that drives scaling. That is, precipitation scaling in the model is entirely determined after specifying a temperature trend and a scenario of precipitation scaling per degree warming. In this way, emerging hypotheses related to regional warming and precipitation-temperature scaling relationships, which are arguably less uncertain than precipitation changes linked to dynamical processes (Pfahl et al., 2017), can be directly tested with respect to their impact on water systems.

3.2. Model Calibration and Validation

The identification and simulation of the WRs (Section 3.1.1) play a critical role in the performance of the weather generator. A key parameter of the model is K , the number of WRs that should be used across the calendar year. To calibrate the value of K , we generated 50 ensemble traces of weather from the weather generator for each of the 20 different HUC8 watersheds under baseline conditions (i.e., no climate change) and for values of K ranging from 2 to 16 WRs. We then evaluated the distribution of a variety of regional climate performance measures across the 20 different watersheds. All performance measures were assessed on basin-averaged precipitation for calibration purposes, and were based on the percent bias between simulated ensemble median and observed statistics of interest. These statistics included:

- Mean daily precipitation
- Standard deviation of annual precipitation
- Probability of dry and wet days
- Average and maximum length of dry and wet spells
- Maximum 1-, 3-, 7-, 10-, 14-, and 30-day precipitation events
- Estimated 2-, 5-, 10-, 20-, 50-, and 100-year 24-hour precipitation events
- Minimum 3-month, 6-month, 1-year, and 2-year precipitation events

No one value of K (i.e., number of WRs) is likely to maximize performance across all these measures for all HUC8 watersheds. Therefore, we selected K based on the value that provided the best balance across all statistics over all watersheds.

After calibrating the value of K and validating model performance, we also considered calibration of one additional free parameter – the threshold of basin average precipitation used to separate dry and wet days. This value (by default set to 0 mm) is important in the resampling algorithm of the weather generator (see Section 3.1.2), but it is possible that a threshold greater than zero would improve resampling properties of the generator algorithm. A similar process to that used to select K was also applied to this parameter.

Following calibration, the final parameterization of the weather generator was then validated for all HUC8 watersheds. Validation involved a similar process to calibration, with two major differences: 1) most performance measures were assessed at individual grid cell locations within each basin, rather than on the basin average, and 2) a larger set of performance statistics was considered beyond those used for calibration. These statistics are listed in Table 3 (for precipitation) and Table 4 (for temperature), along with their abbreviated name and short description. We note that many of these statistics are not reported as final outputs of the weather generator that are made available to the public through the Resilient MA website, but rather are used only for internal validation of the model.

Table 3. Statistics of precipitation used for model validation.

No	Abbreviated Name	Statistic [unit]
1	mean	Daily precipitation mean (mm)
2	sd	Daily precipitation standard deviation (mm)
3	skew	Daily precipitation skew (-)
4	cross.correlation	Rank correlation of daily precipitation across all grid cells within a basin (-)
5	annual.sd	Standard deviation of annual mean of daily precipitation across years (mm)
6	annual.skew	Skew of annual average precipitation across years (-)
	basin.monthly.means	Monthly mean of daily average precipitation for the basin average (mm)
7	basin.annual.sd	Standard deviation of annual average precipitation across years for the basin average (mm)
8	basin.annual.skew	Skew of annual average precipitation across years for the basin average (-)
9	prob.dry.days	The probability of a dry day (i.e., 0 mm of precipitation) (-)
10	prob.wet.days	The probability of a wet day (i.e., > 0 mm of precipitation) (-)
11	mean.dry.spell.length	The average length of a dry spell (i.e., consecutive dry days) (days)
12	mean.wet.spell.length	The average length of a wet spell (i.e., consecutive wet days) (days)
13	max.dry.spell.length	The maximum length of a dry spell (i.e., consecutive dry days) (days)
14	max.wet.spell.length	The maximum length of a wet spell (i.e., consecutive wet days) (days)
15	1.day.max	The maximum 1-day precipitation value in the entire record (mm)
16	3.day.max	The maximum 3-day average precipitation value in the entire record (mm)
17	7.day.max	The maximum 7-day average precipitation value in the entire record (mm)
18	10.day.max	The maximum 10-day average precipitation value in the entire record (mm)
19	14.day.max	The maximum 14-day average precipitation value in the entire record (mm)
20	30.day.max	The maximum 30-day average precipitation value in the entire record (mm)
21	2-yr.return.level.max	The 2-year return level event, estimated from a GEV distribution fit to annual maxima (mm)
22	5-yr.return.level.max	The 5-year return level event, estimated from a GEV distribution fit to annual maxima (mm)

23	10-yr.return.level.max	The 10-year return level event, estimated from a GEV distribution fit to annual maxima (mm)
24	20-yr.return.level.max	The 20-year return level event, estimated from a GEV distribution fit to annual maxima (mm)
25	50-yr.return.level.max	The 50-year return level event, estimated from a GEV distribution fit to annual maxima (mm)
26	100-yr.return.level.max	The 100-year return level event, estimated from a GEV distribution fit to annual maxima (mm)
27	7.day.min	The lowest 7-day average daily precipitation amount in the record (mm)
28	1.month.min	The lowest 1-month average daily precipitation amount in the record (mm)
29	3.month.min	The lowest 3-month average daily precipitation amount in the record (mm)
30	6.month.min	The lowest 6-month average daily precipitation amount in the record (mm)
31	1.year.min	The lowest 1-year average daily precipitation amount in the record (mm)
32	2.year.min	The lowest 2-year average daily precipitation amount in the record (mm)
33	90th.percentile	The 90 th percentile of the daily precipitation (mm)
34	99th.percentile	The 99 th percentile of the daily precipitation (mm)
35	consecutive.dry.days	The average number of days that exist within a run of 2 or more dry days (days)
36	consecutive.wet.days	The average number of days that exist within a run of 2 or more wet days (days)
37	prob.dry.to.wet	The probability that a dry day transitions to a wet day (-)
38	prob.wet.to.dry	The probability that a wet day transitions to a dry day (-)
39	days.above.1.inch	The number of days with precipitation greater than 1 inch (days)
40	days.above.2.inch	The number of days with precipitation greater than 2 inches (days)
41	days.above.4.inch	The number of days with precipitation greater than 4 inches (days)

Table 4. Statistics of temperature used for model validation.

No	Abbreviated Name	Statistic [unit]
1	mean	Daily average temperature mean (°C)
2	sd	Daily average temperature standard deviation (°C)
3	skew	Daily average temperature skew (-)
4	min	The minimum daily average temperature value in the entire record (°C)
5	max	The maximum daily average temperature value in the entire record (°C)
6	lag1.cor	Lag-1 autocorrelation of daily average temperature (-)
7	annual.sd	Standard deviation of the annual mean of daily average temperature across years (°C)
8	annual.skew	Skew of the annual mean of daily average temperature across years (°C)
9	cross.correlations	Rank correlation of daily temperature across all grid cells within a basin (-)
10	basin.monthly.means	Monthly mean of daily average temperature for the basin average (°C)

11	basin.seasonal.sd	Standard deviation of the annual mean of daily average temperature for the basin average (°C)
12	basin.seasonal.skew	Skew of the annual mean of daily average temperature for the basin average (-)
13	number.heatwaves	Number of instances with three or more consecutive days with temperature over 90°F (-)
14	number.coldwaves	Number of instances with ten or more consecutive days with temperature below 20°F (-).
15	mean.heatwaves.duration	Average duration of heatwaves (days)
16	mean.coldwaves.duration	Average duration of coldwaves (days)
17	max.heatwaves.duration	Longest duration of heatwaves in the record (days)
18	max.coldwaves.duration	Longest duration of coldwaves in the record (days)

3.3. Thermodynamic Scenario Development

In this section, we provide detail on the specific climate change scenarios developed through this work. All climate scenarios are designed to reflect thermodynamic processes only.

For every HUC8 watershed in Massachusetts, we generated 50 ensemble members, each 64-years long (the length of the instrumental record), for temperature changes that range from 0°C to 8°C warming at 0.5°C increments. This is the range of warming projected by the MACA-downscaled CMIP5 dataset across the state of Massachusetts described in Section 2.2. In Section 4.3 below, we demonstrate how these scenarios can be used in conjunction with temperature projections from an ensemble of GCM projections to update the data on the Resilient MA website.

To scale the 99.9th percentile of non-zero precipitation in the quantile mapping procedure described in Section 3.1.3, we use the theoretical Clausius-Clapeyron (CC) scaling rate (~7% per °C warming; Alduchov & Eskridge (1996)). If all other factors controlling precipitation intensity remain unchanged, it is often assumed that extreme precipitation will scale with temperature at this same rate (Allen & Ingram 2002; Allan & Soden, 2008). The reasoning is that under conditions that lead to extreme precipitation (i.e., near saturated atmospheric conditions; intense surface convergence and uplift), changes in atmospheric moisture content will translate directly to changes in precipitation amount. A separate analysis of extreme precipitation scaling conducted under this Phase I project and a survey of the literature for daily temperature-precipitation scaling supports this choice (Trenberth, 2011; Westra et al., 2014; Fischer and Knutti, 2016; Bao et al., 2017; Lenderink et al., 2017; Guerreiro et al., 2018).

For mean precipitation, we did not apply any scaling with temperature (i.e., 0% per °C warming). Empirical evidence from multi-model ensembles (Emori and Brown, 2005; Li et al., 2013; Hawcroft et al., 2018) highlights constraints on mean precipitation thermodynamic scaling due to limiting rates of atmospheric cooling (Allen and Ingram, 2002; Muller and O’Gorman, 2011; Pendergrass and Hartmann, 2014b) over land in the midlatitudes. In addition, some studies suggest that thermodynamically driven declines in mean precipitation are possible over land due to changes in atmospheric water vapor gradients that could reduce moisture convergence (Ting et al., 2018). Without an in-depth analysis of these mechanisms for the Northeast US, which was beyond the scope of this work, a choice was made to only allow extreme precipitation to scale with temperature and to maintain mean precipitation at historical levels in all future scenarios developed in this work.

Finally, we reiterate here that mechanisms of dynamic climate change were not addressed in this Phase I effort. However, future work could develop scenarios of dynamic climate change through the perturbation of WR frequencies within the NHMM, through adjustments to the transition probability matrix used to drive its simulations. These adjustments would be based off an assessment of GCM-based projections of WR frequencies.

4. Results

4.1. Model Calibration

In Figures 2-5 below, we show the distribution of percent bias (Gupta et al., 1998) between simulated ensemble median and observed values for a variety of performance statistics. The x-axis of each panel shows the number of WRs (i.e., value of K) being tested, and the y-axis shows the distribution of percent bias across the 20 different HUC8 watersheds. For calibration, all bias statistics are being shown for the basin averaged precipitation value. We focus on moments and spell lengths in Figure 2, multi-day precipitation maxima in Figure 3, return period events in Figure 4, and drought events in Figure 5.

Figures 2-5 show that no one value of K optimizes performance across all calibration metrics. For example, a 9-WR model minimizes bias across the 20 HUC8 watersheds for mean precipitation, while a 7-WR model minimizes bias for the annual standard deviation of precipitation. However, these models have very large biases in other statistics of interest, including probability of dry and wet days and the maximum length of wet and dry spells (Figure 2).

Looking across all metrics (Figures 2-5), a few key patterns emerge. First, the percent bias varies between -15% and +15% over most of statistics and different WRs selections, suggesting that most versions of the model perform reasonably well across a host of precipitation characteristics. Second, biases in average spell lengths tend to become larger for $K > 12$, while biases in maximum spell lengths are larger for $K \leq 10$ (see Figure 2). Third, a larger number of WRs ($10 \leq K \leq 14$) exhibits less percent bias across different x-day maximum precipitation statistics (Figure 3). Similarly, when $11 \leq K \leq 14$, percent bias is reduced for different return level events (Figure 4). Finally, short-duration droughts (especially at a 3-month length) are better estimated with a larger number of weather regimes, while drought magnitudes tend to be positively biased (too wet) regardless of K at the longest durations.

Ultimately, based on the results in Figures 2-5 we decided that $K=12$ WRs provided the best overall performance across the range of statistics tested. In addition, further tests (not shown) suggested that model performance was highly insensitive to the threshold of precipitation used to distinguish between dry and wet days in the block bootstrap module of the algorithm. Therefore, this value was retained at its default value (0 mm).

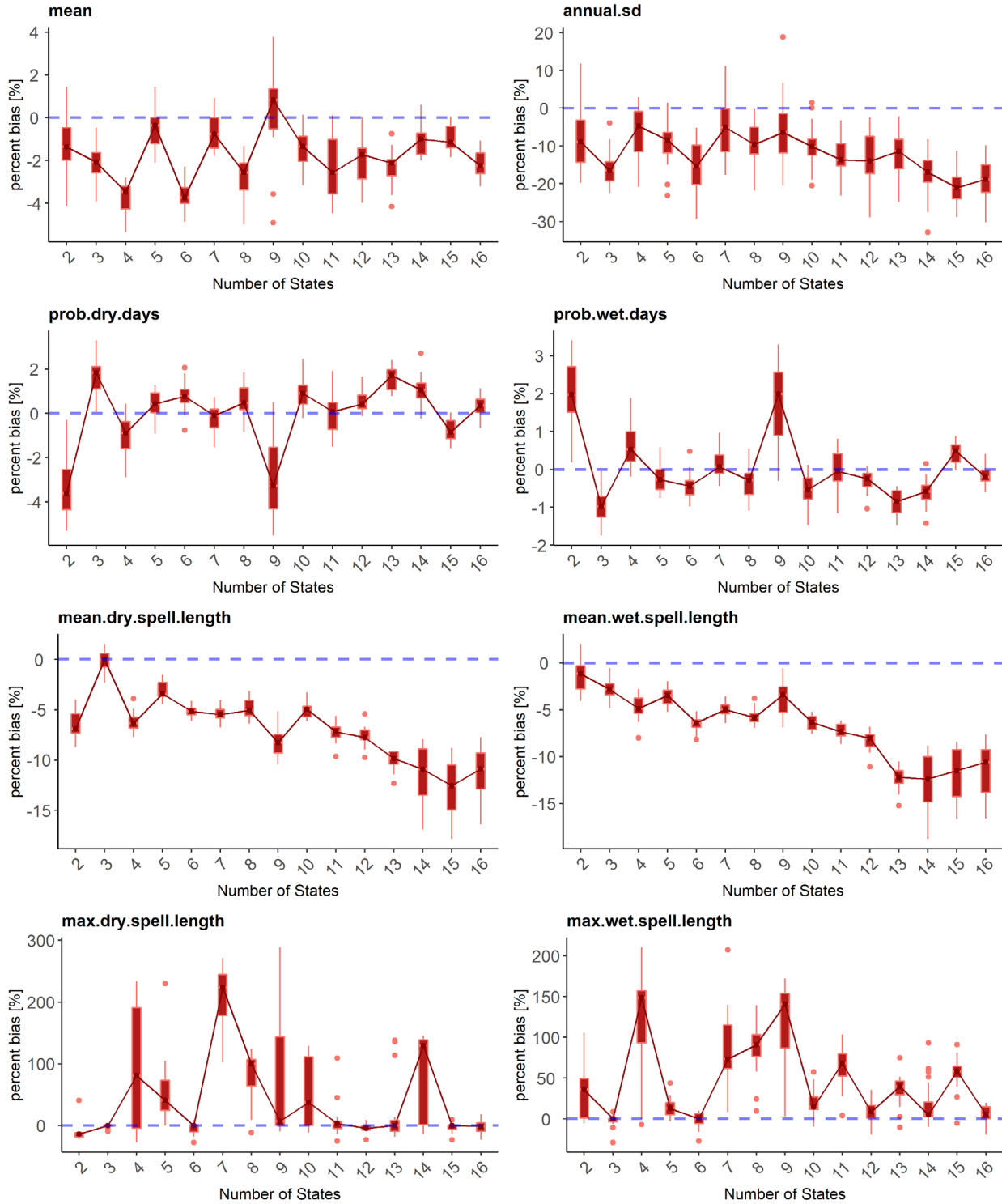


Figure 2. Distribution of percent bias between simulated ensemble median and observed values across 20 HUC8 watersheds for performance statistics including daily mean precipitation, annual standard deviation of precipitation, probability of wet and dry days, and both average and maximum length of wet and dry spells. Percent bias distributions are shown for weather generator simulations using 2-16 number of WRs and the basin averaged precipitation value.

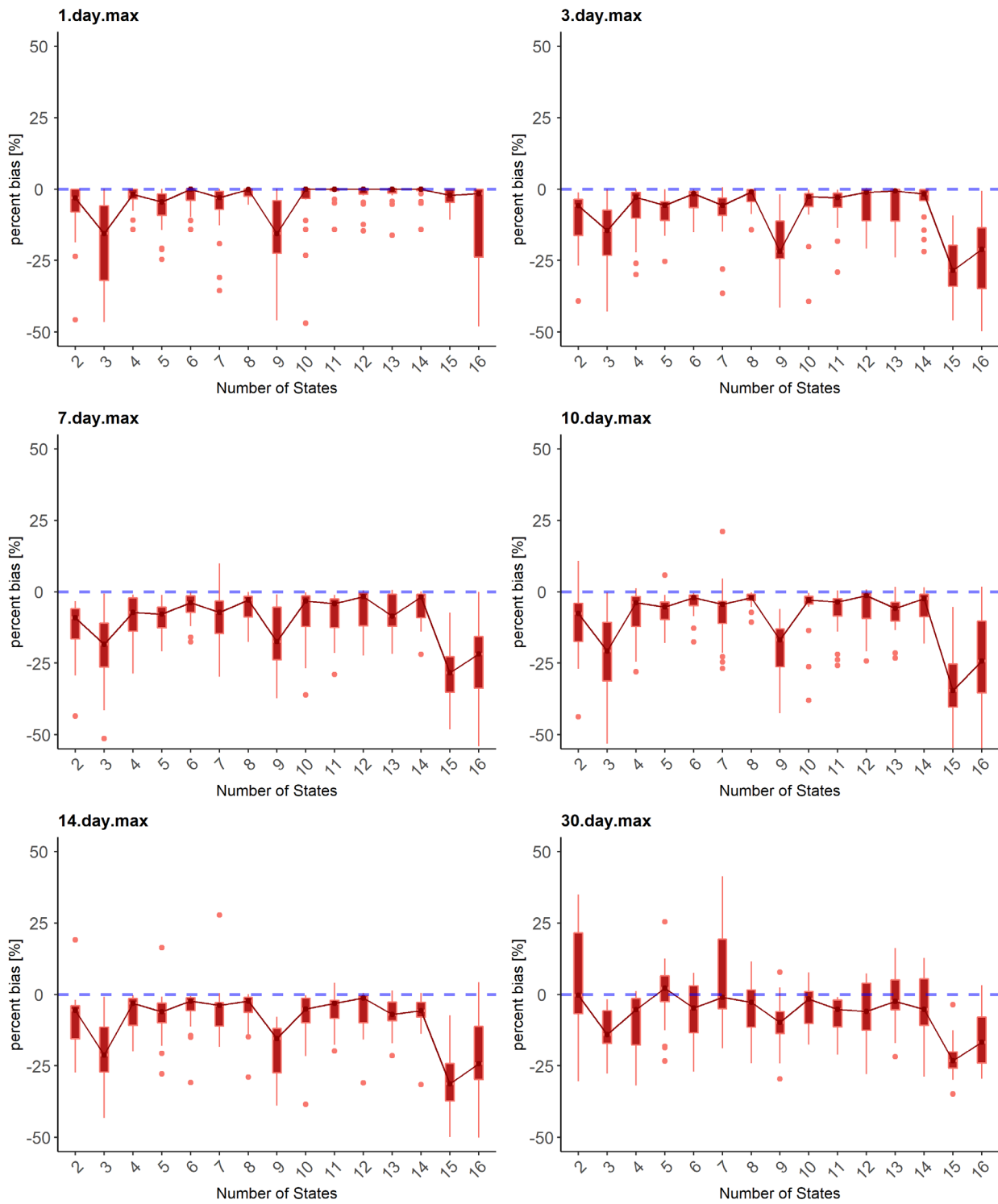


Figure 3. Same as Figure 2, but for the 1-, 3-, 7-, 10-, 14-, and 30-day maximum precipitation events.

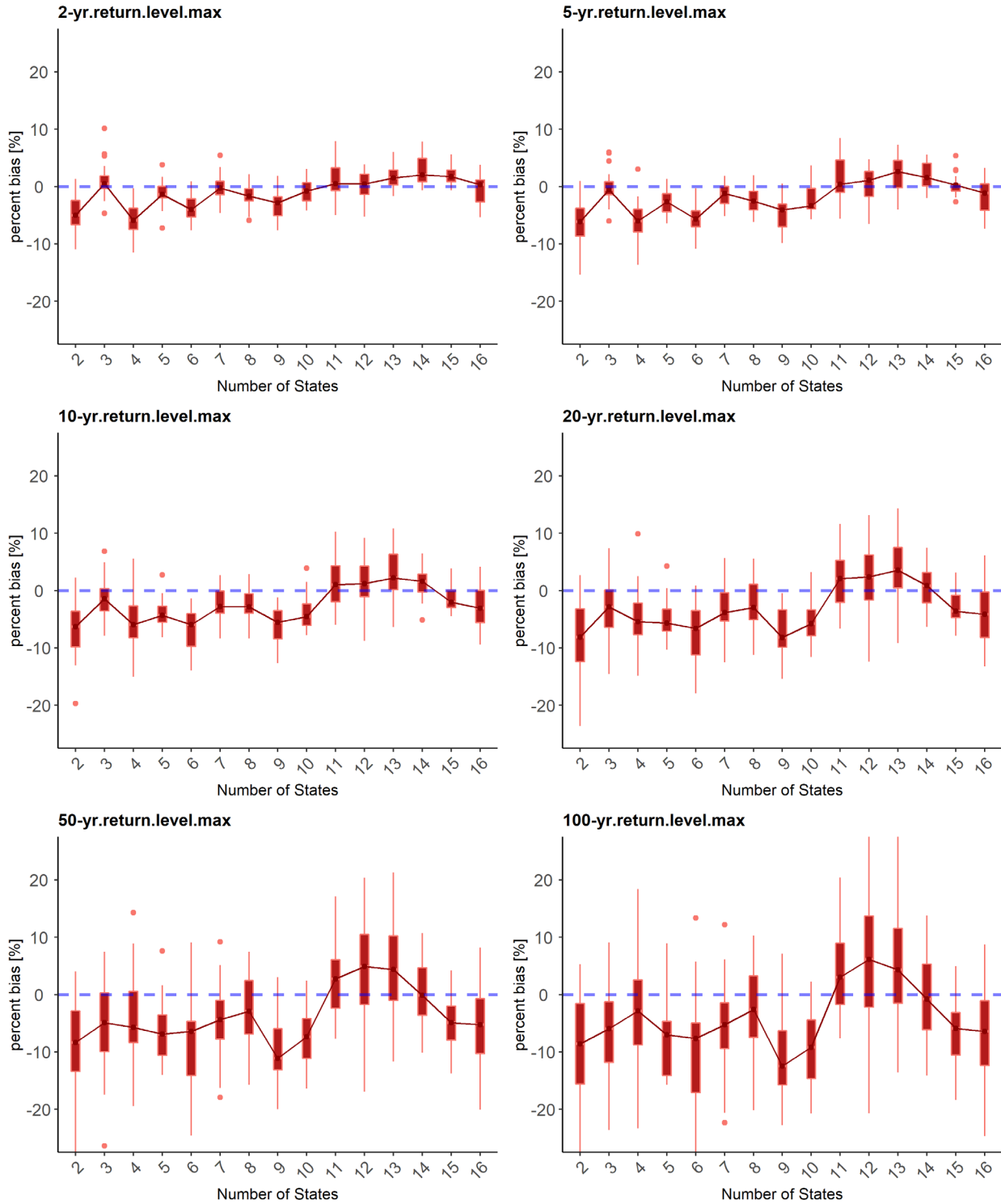


Figure 4. Same as Figure 2, but for the estimated 2-, 5-, 10-, 20-, 50-, and 100-year precipitation event.

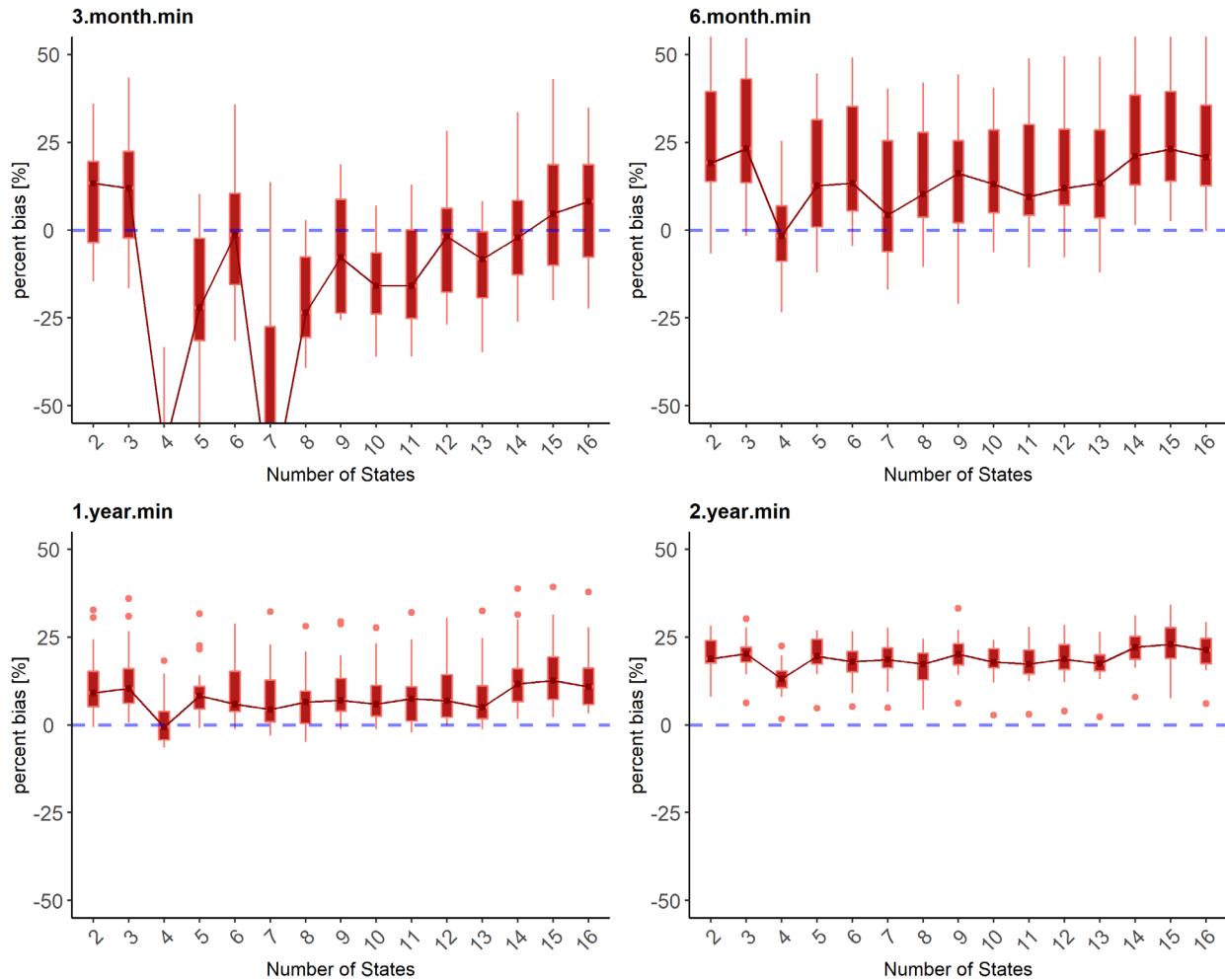


Figure 5. Same as Figure 2, but for the minimum 3-month, 6-month, 1-year, and 2-year precipitation events.

Figure 6 shows the spatial distribution of a subset of performance statistics across the HUC8 watersheds using the final parameterization of our weather generator ($K=12$). Overall, there are limited spatial patterns in weather generator performance, albeit with a few exceptions. For example, the daily maximum precipitation metric shows a slight negative bias over basins near the coastline, the 1-year drought metric is more biased in the western half of the state, and the annual standard deviation is more biased for northern and northeastern watersheds. However, most other statistics generally exhibit consistent bias across all watersheds, suggesting relatively uniform model performance regardless of location.

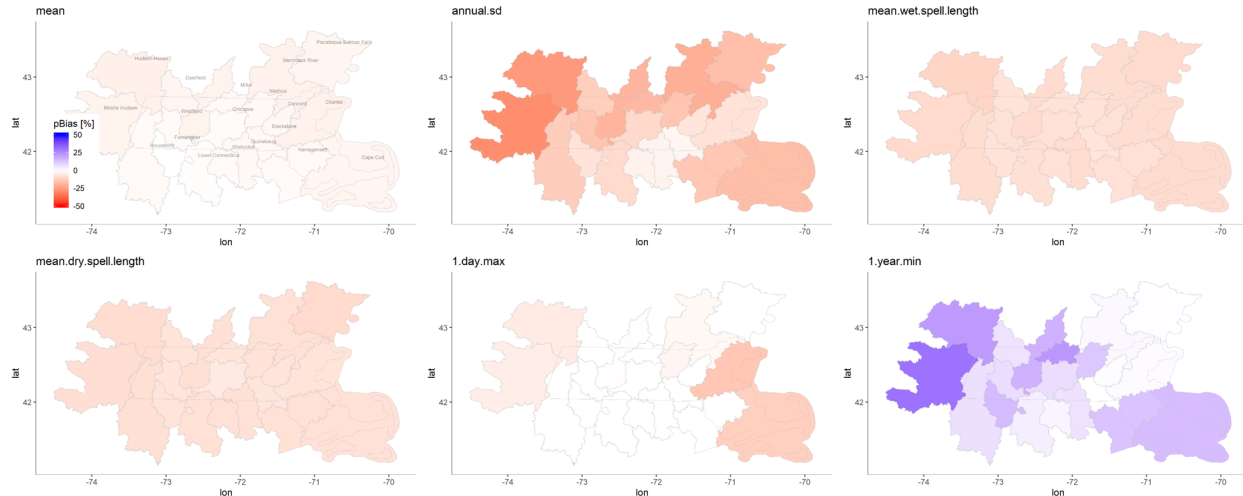


Figure 6. The spatial distribution of percent bias across the 20 different HUC8 watersheds for mean daily precipitation, the annual standard deviation of precipitation, the average length of dry and wet spells, the maximum precipitation value, and the minimum of 1-year rolling average precipitation.

Finally, we show the 12 different weather regimes that were identified for the stochastic weather generator (Figure 7). These WRs emphasize patterns of atmospheric flow with varying levels of intensity and spatial orientations around the Northeast US. They are often characterized by a lobe of low or high pressure over the Northeast, or a dipole of high and low pressure that straddle the Northeast. Many of these patterns are part of larger wave trains emanating out of the Pacific/North American sector.

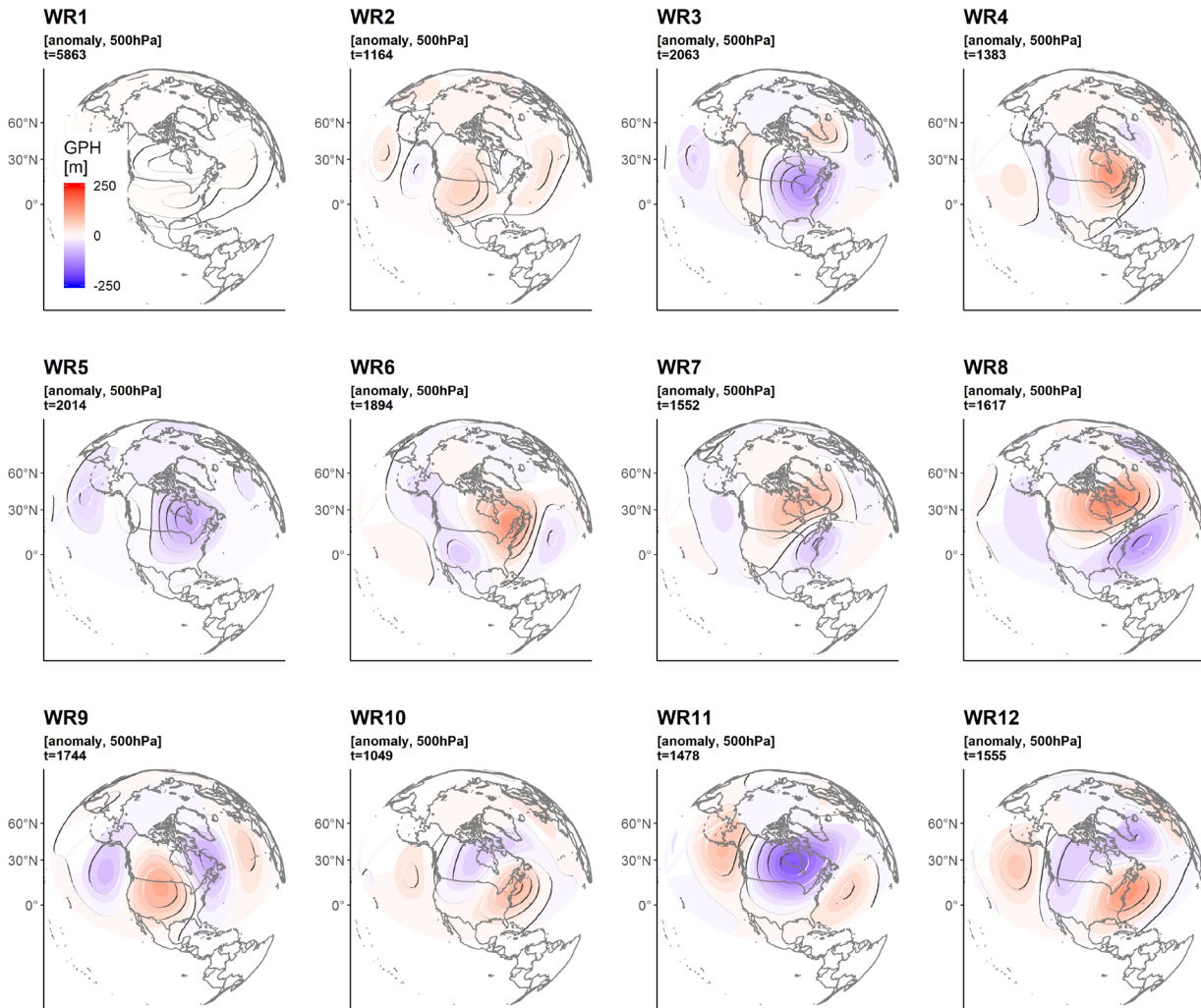


Figure 7. Composites of 500-hPa geopotential height (GPH) anomalies for all days classified into one of the 12 WRs. Number of days in the record classified into each WR is also shown.

4.2. Model Validation

Figures 8 and 9 show a variety of observed and simulated precipitation statistics (see Table 3) for the Nashua River basin, most on an at-site (i.e., grid cell) basis. Many of these statistics were not considered during calibration, and thus provide additional validation of the model. The spread around simulated statistics from an ensemble of 50 weather generator traces is also shown. Performance for temperature statistics (see Table 4) is shown in Figures 10 and 11 for both maximum and minimum temperature. In the Appendix, similar figures are shown for three other HUC8 watersheds (the Concord, Blackstone, and Westfield).

Figure 8 shows that most of the characteristics of precipitation intensity, including the mean, standard deviation, maximum, basin-wide monthly means, and probability of dry and wet days, are well simulated, with observed statistics falling within the range simulated by the weather generator ensemble. In addition, there is little spatial variation in performance within the Nashua Basin, with all grid cells showing similar performance. A few statistics such as average spell lengths are underestimated, but the difference between observed and simulated average spell

lengths is less than half a day. In addition, the observed maximum spell lengths are well captured within the model spread. This suggests the model results are likely adequate for hydrologic simulation, especially with respect to extreme events driven by long-duration wet and dry spells.

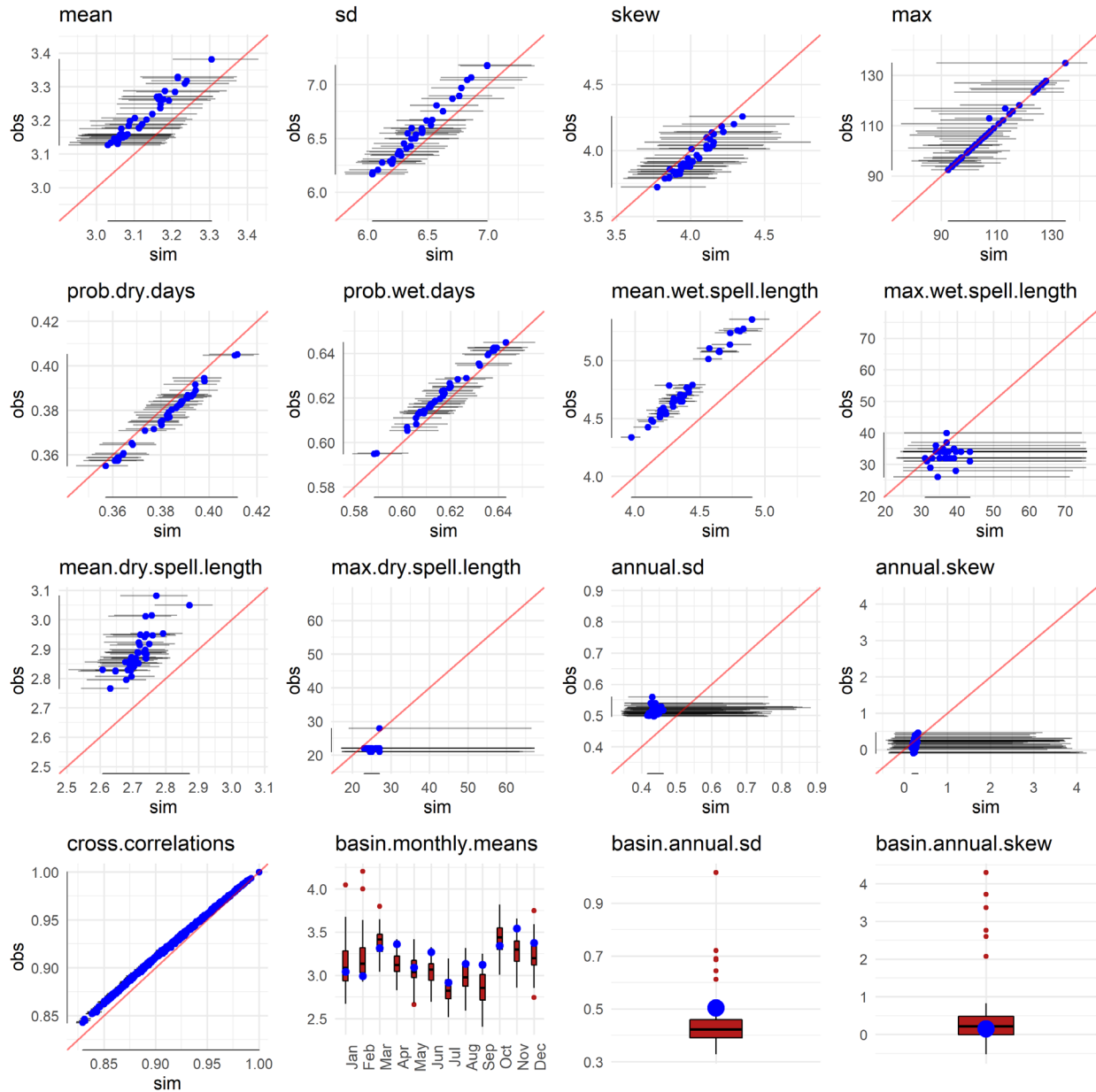


Figure 8. Observed vs. simulated characteristics of daily precipitation in the Nashua Basin (see Table 3 for description of statistics). For at-site characteristics, each simulated point represents the median performance metric across 50 ensemble members at a gridded location within the basin. The thin horizontal lines (whiskers) denote the 95% range for simulated metrics across the ensemble. For basin-averaged statistics, the distribution of simulated statistics is shown as a boxplot along with the observed value.

Figure 9 shows metrics that quantify the characteristics of extreme precipitations, such as the x-day maximum of precipitation, different durations of precipitation deficit, 24-hour return periods,

different percentiles of the precipitation distribution, and days with precipitation above a high threshold. In general, most of these statistics show good to very good agreement with the observations, including all return period events, precipitation percentiles, and the number of days with very high precipitation. There are a few larger biases related to the median weather generator simulation for certain x-day maximum precipitation events and more extended periods of minimum precipitation, although the observed statistics often fall within the range simulated by the weather generator ensemble. Overall, these results suggest that the weather generator can capture many characteristics of extreme precipitation within an ensemble of simulations.

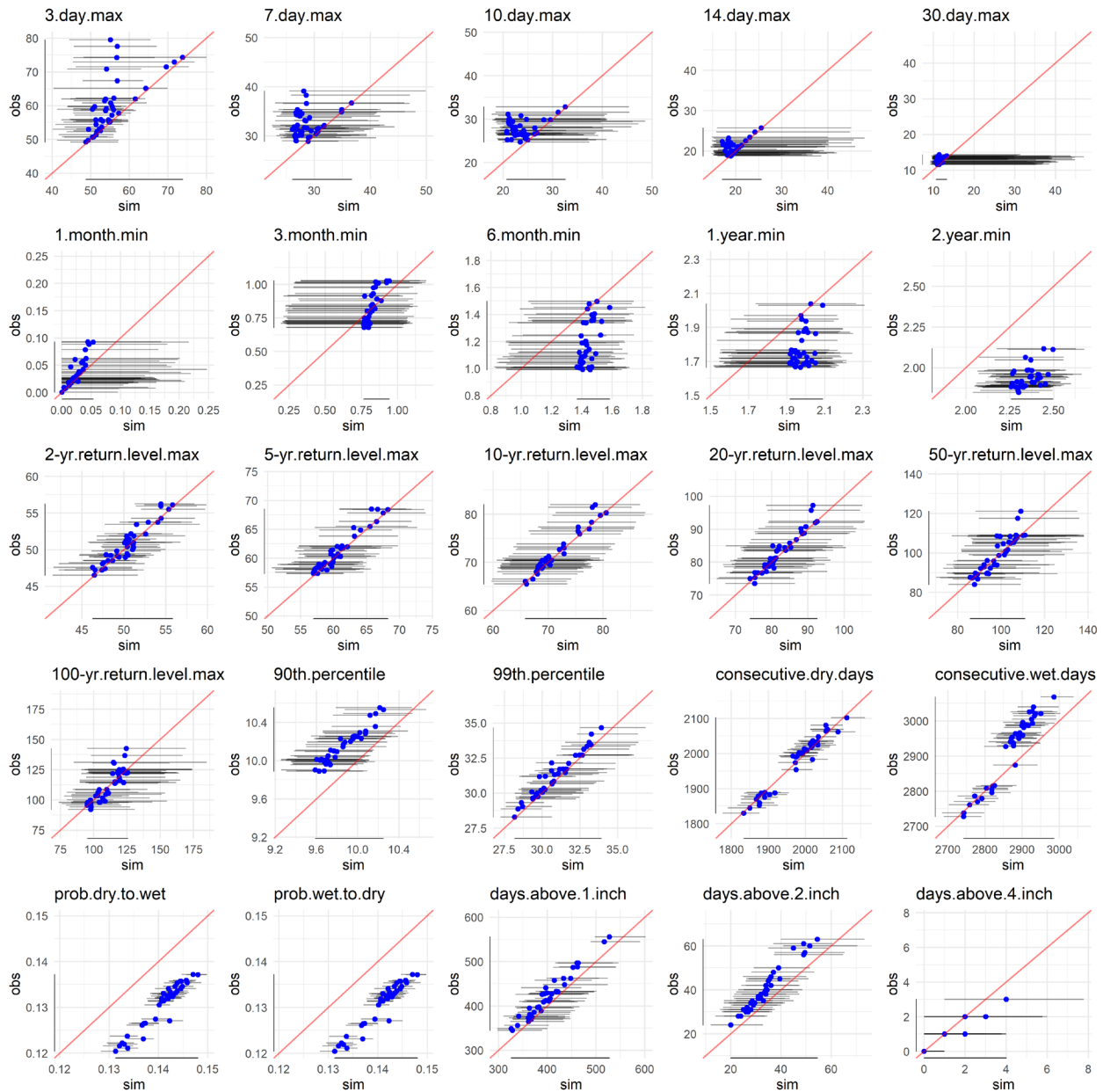


Figure 9. Same as Figure 8, but for characteristics of extreme precipitation, including multi-day maximum and minimum precipitation magnitudes, daily precipitation return levels estimated based on a GEV distribution fit to annual maxima, percentiles of the precipitation distribution, the number of days

within dry and wet spell runs, transition probabilities between dry and wet days, and days with precipitation above different high thresholds (see Table 3).

Figure 10 shows statistics for validating simulated maximum and minimum temperature. Almost all statistics highlight good to very good performance in simulations of different temperature statistics, including moments of the daily, monthly, and annual distribution and spatial correlation across sites. Performance is also very consistent across grid cells. The weather generator does moderately underestimate persistence in temperature (downward bias in the lag-1 autocorrelation), but the magnitude of this bias is not large.

Figure 11 highlights characteristics related to temperature extremes, including heatwaves, heat stress, coldwaves, and cold stress. Model performance is very good for most of these statistics, especially with respect to heatwaves and heat stress. There is a moderate downward bias in the number and duration of coldwaves, but the observed statistics do tend to fall towards the outer range of the simulated ensemble. Overall, there is a high level of agreement between the observed and simulated statistics of average and extreme temperature using the weather generator.

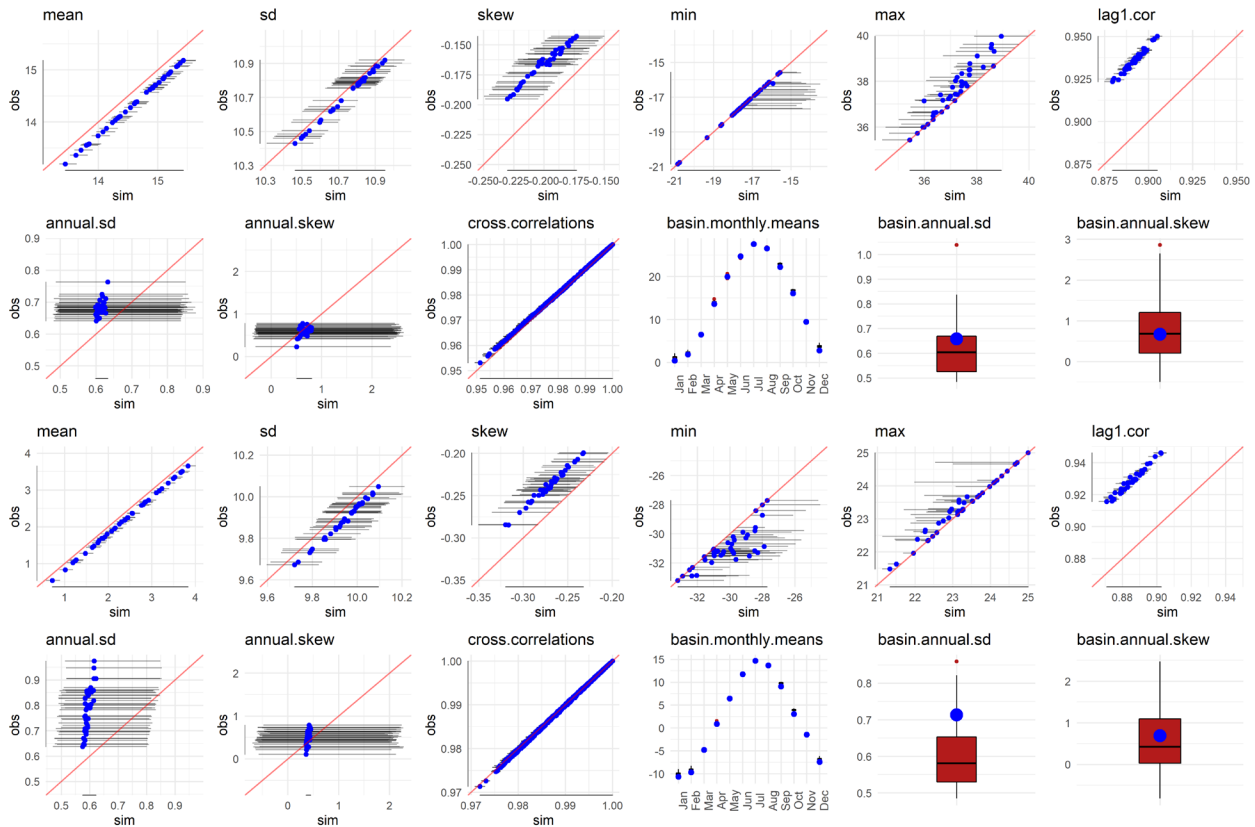


Figure 10. Observed vs. simulated characteristics of daily maximum (first two rows) and minimum (second two rows) temperature in the Nashua Basin (see Table 4 for description of statistics). For at-site characteristics, each simulated point represents the median performance metric across 50 ensemble members at a gridded location within the basin. The thin horizontal lines (whiskers) denote the 95% range for simulated metrics across the ensemble. For basin-averaged statistics, the distribution of simulated statistics is shown as a boxplot along with the observed value.

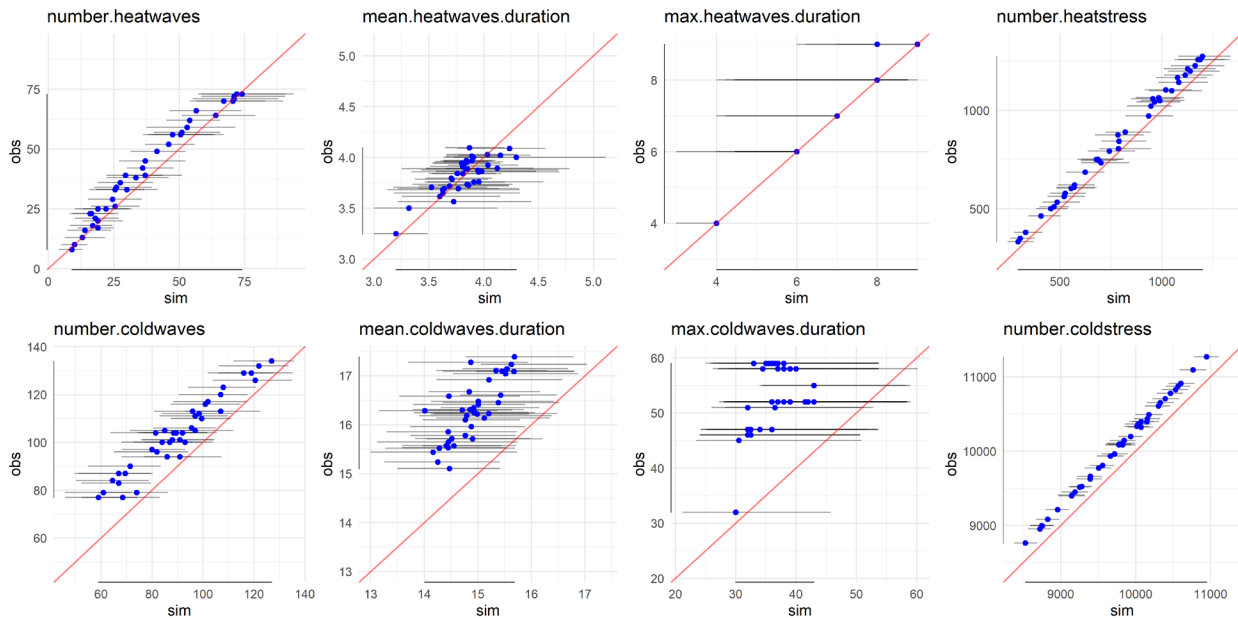


Figure 11. Same as Figure 10, but for temperature statistics related to heatwaves (based on maximum temperature) and coldwaves (based on minimum temperature) (see Table 4).

4.3. Demonstration of Thermodynamic Climate Change Scenarios

The stochastic weather generator was run under 17 different temperature scenarios, from 0° to 8°C warming at 0.5° increments. Each run consisted of 50 ensemble member simulations for that scenario of change. For each ensemble member, we calculated a set of temperature and precipitation statistics to be included in the final deliverable for the Resilient MA website. These statistics are listed in Table 5.

Table 5. List of statistics calculated for Resilient MA. The units of change represent how changes in these statistics for future target decades are presented on Resilient MA, as compared to baseline values. *Note: Total precipitation can be converted to mean daily precipitation for the year or season by dividing by the number of days in a year (365) or season (90 or 91).

No.	Precipitation	Units of Change	Temperature	Units of Change	
1	Consecutive dry days	# days	1	Average temperatures	°F
2	Consecutive wet days	# days	2	Maximum temperatures	°F
3	Extreme precipitation > 1 in	# days	3	Minimum temperatures	°F
4	Extreme precipitation > 2 in	# days	4	Cooling degree days	degree-day
5	Extreme precipitation > 4 in	# days	5	Growing degree days	degree-day
6	Total precipitation*	% change	6	Heating degree days	degree-day
7	Maximum precipitation	% change	7	Days < 0 F	# days
8	90th percentile of precipitation	% change	8	Days < 32 F	# days
9	99th percentile of precipitation	% change	9	Days > 100 F	# days
10			10	Days > 90 F	# days
11			11	Days > 95 F	# days
12			12	Number of heatwaves	# events

13		13	Average duration of heatwaves	# days
14		14	Maximum duration of heatwaves	# days
15		15	Number of coldwaves	# events
16		16	Average duration of coldwaves	# days
17		17	Maximum duration of coldwaves	# days
18		18	Number of heatstress events	# events
19		19	Number of coldstress events	# events

For each statistic, a baseline value is calculated based on the median value for the statistic across the 50 ensemble members associated with the 0°C temperature change scenario. These statistics are calculated for basin average precipitation or basin average temperature, as the final statistics reported on Resilient MA are shown at the HUC8 level. The baseline value is then compared against similarly calculated values for each of the 16 other warming scenarios (0.5°, 1.0°, 1.5°, ..., 8°C). The change between statistics calculated for a warming scenario and the baseline is then recorded. This change is reported either as a percent or absolute difference, depending on the metric (e.g., changes in average temperature are reported as absolute differences in degrees Fahrenheit; changes in total precipitation are reported as a percent difference; changes in the number of days or instances a certain event occurs are presented as an absolute number of days or events). The units of change for all statistics are shown in Table 5. As a result, each of the different scenarios of temperature change run through the stochastic weather generator is associated with a set of delta changes for precipitation and temperature statistics of interest.

Ultimately, these delta changes are reported for target decades (2030, 2050, 2070, 2090) for each HUC8 watershed. To do this, we calculate 30-year average temperature changes for the ensemble of MACA-downscaled GCM projections around each of those target decades (we use a 20-year window for the 2090's due to data limitations): [2020-2049] for 2030; [2040-2069] for 2050; [2060-2089] for 2070; and [2080-2099] for 2090. This is done both at the annual scale, and for specific seasons. The result is a distribution of (annual and seasonal) temperature changes for each target decade, where the distribution is composed of the 20 different model projections. We then calculate the median of this distribution, as well as the 10th and 90th percentile. The final temperature changes calculated at the annual timescale under RCP 8.5 are shown for each basin in Table 6, with temperature changes by season shown in the Appendix.

For each of the three percentile values (the 10th, 50th, and 90th), we find the nearest temperature change scenario developed using the stochastic weather generator, and extract the delta change for precipitation and temperature statistics associated with those weather generator scenarios. In this way, time-varying projections of warming from the GCMs are mapped to changes in precipitation and temperature statistics developed using the weather generator. An example result for this process is shown in Tables 7, 8, and 9. These results show one precipitation statistic of interest for the Nashua basin: the number of days in a basin that have greater than 1 inch of precipitation. For that statistic calculated at both annual and seasonal timescales, the baseline value is reported based on weather generator simulations without any temperature increase. For instance, at the annual scale, the weather generator simulates (on average) about 5.13 days per year with precipitation greater than 1 inch. In the four different seasons, the number of days ranges between 1.08 and 1.81

days per season. Across the 20 different climate model projections, the median annual average temperature increase under RCP 8.5 for 2090 was 5.66°C (see Table 6, basin no. 11). This value is closest to the 5.5° warming scenario generated using the weather generator, and so the delta change for this precipitation statistic is retrieved from that weather generator scenario and reported in Table 7. In this case, we report that there will be 2.13 more days with precipitation greater than 1 inch per year compared to the baseline value of 5.13 days (i.e., there will be 7.26 days with precipitation greater than 1 inch per year on average by the 2090s; see uppermost right cell in Table 7).

Table 6. The 10th percentile, median (50th percentile), and 90th percentile of temperature changes (°C) across all 20 GCMs under RCP 8.5 at an annual scale for the target decades of 2030, 2050, 2070, and 2090. Results are shown for each of the 20 HUC8 basins (see Table 1; the Nashua is basin #11).

RCP 8.5												
Annual	2030s			2050s			2070s			2090s		
basin no.	10th	50th	90th									
1	1.20	2.04	2.99	2.23	3.32	4.58	3.32	4.72	6.40	4.10	5.77	7.69
2	1.27	2.08	3.00	2.25	3.37	4.54	3.33	4.78	6.27	4.06	5.83	7.58
3	1.16	1.89	2.76	2.12	3.07	4.20	3.09	4.33	5.73	3.88	5.27	6.85
4	1.20	1.96	2.86	2.18	3.17	4.37	3.17	4.49	6.02	3.95	5.47	7.19
5	1.29	2.03	2.90	2.24	3.26	4.39	3.23	4.58	5.98	4.00	5.57	7.20
6	1.20	1.92	2.79	2.17	3.15	4.29	3.19	4.48	5.87	4.00	5.46	7.06
7	1.25	1.95	2.83	2.20	3.16	4.29	3.17	4.45	5.82	3.97	5.41	6.98
8	1.27	2.04	2.95	2.25	3.32	4.48	3.30	4.72	6.16	4.08	5.76	7.47
9	1.22	1.94	2.83	2.17	3.16	4.32	3.18	4.48	5.89	3.98	5.45	7.08
10	1.26	2.02	2.90	2.22	3.25	4.38	3.24	4.59	5.99	4.00	5.59	7.23
11	1.24	2.02	2.95	2.22	3.28	4.46	3.27	4.64	6.17	4.04	5.66	7.45
12	1.21	1.96	2.87	2.19	3.21	4.40	3.22	4.55	6.07	4.02	5.55	7.28
13	1.24	2.02	2.95	2.24	3.32	4.50	3.33	4.74	6.25	4.11	5.79	7.59
14	1.26	2.01	2.93	2.21	3.26	4.42	3.26	4.62	6.09	4.03	5.63	7.35
15	1.08	1.86	2.70	2.05	3.00	4.09	2.98	4.21	5.58	3.73	5.10	6.69
16	1.22	2.05	3.00	2.23	3.32	4.54	3.31	4.71	6.30	4.08	5.75	7.62
17	1.26	2.05	2.97	2.25	3.35	4.52	3.33	4.77	6.27	4.11	5.83	7.63
18	1.31	2.15	3.12	2.29	3.45	4.65	3.36	4.88	6.46	4.11	5.95	7.85
19	1.23	1.96	2.85	2.18	3.16	4.33	3.17	4.46	5.90	3.96	5.43	7.06
20	1.26	2.06	2.98	2.26	3.38	4.54	3.33	4.82	6.33	4.10	5.89	7.71

To account for uncertainty in the GCM-based temperature projections, we also consider the 90th and 10th percentile of the 20 GCM projections of annual mean temperature around the target year of 2090. These percentiles of temperature increase under RCP 8.5 are 4.04°C and 7.45°C, which are closest to the 4° and 7.5° warming scenarios generated using the weather generator. The delta changes for precipitation days greater than 1 inch are retrieved from these weather generator scenarios and are shown in the uppermost right cell of Tables 8 and 9, respectively. Using the 90th percentile (10th percentile) of GCM-projected temperature increase, we report that there will be 2.83 (1.60) more days with precipitation greater than 1 inch per year compared to the baseline value of 5.13 days. Similar results are shown for all seasons and target years.

Table 7. Projected change in the number of days with greater than 1 inch of precipitation, for the full year and by season for the Nashua Basin. The Baseline shows the average number of days per year with greater than 1 inch of precipitation in baseline runs of the weather generator (i.e., no thermodynamic climate change). Columns labeled 2030, 2050, 2070, and 2090 show the change in the number of days over the baseline, based on weather generator simulations with temperature increases corresponding to the median temperature increase projected by an ensemble of MACA-downscaled GCMs. Results are shown for the RCP 8.5 scenario.

Season	Baseline	Emission Scenario	2030	2050	2070	2090
<i>Annual</i>	5.13	RCP8.5	0.78	1.41	1.81	2.13
<i>Fall</i>	1.81	RCP8.5	0.26	0.41	0.52	0.64
<i>Spring</i>	1.13	RCP8.5	0.16	0.23	0.32	0.41
<i>Summer</i>	1.08	RCP8.5	0.17	0.30	0.38	0.49
<i>Winter</i>	1.16	RCP8.5	0.18	0.34	0.51	0.63

Table 8. Same as Table 7, but based on weather generator simulations with temperature increases corresponding to the 90th percentile of temperature increases projected by an ensemble of MACA-downscaled GCMs.

Season	Baseline	Emission Scenario	2030	2050	2070	2090
<i>Annual</i>	5.13	RCP8.5	1.20	1.81	2.30	2.83
<i>Fall</i>	1.81	RCP8.5	0.36	0.45	0.68	0.80
<i>Spring</i>	1.13	RCP8.5	0.23	0.36	0.48	0.62
<i>Summer</i>	1.08	RCP8.5	0.22	0.38	0.55	0.63
<i>Winter</i>	1.16	RCP8.5	0.28	0.46	0.67	0.76

Table 9. Same as Table 7, but based on weather generator simulations with temperature increases corresponding to the 10th percentile of temperature increases projected by an ensemble of MACA-downscaled GCMs.

Season	Baseline	Emission Scenario	2030	2050	2070	2090
<i>Annual</i>	5.13	RCP8.5	0.40	0.78	1.41	1.60
<i>Fall</i>	1.81	RCP8.5	0.21	0.30	0.41	0.52
<i>Spring</i>	1.13	RCP8.5	0.06	0.16	0.23	0.26
<i>Summer</i>	1.08	RCP8.5	0.13	0.22	0.26	0.34
<i>Winter</i>	1.16	RCP8.5	0.15	0.23	0.34	0.46

Figure 12 shows the projected change in the number of days with greater than 1 inch of precipitation for the full year (annual) over all the 20 HUC8 watersheds across Massachusetts for the 2050s projection horizon, as an example. The absolute value of this statistic is shown for the Baseline (top row), while changes in this statistic are shown for RCP 8.5 in the bottom row. We show results here for median temperature changes projected by the GCMs (see Table 6). Across the HUC8 watersheds, the number of days with greater than 1 inch of precipitation for the full year ranges between approximately 2 and 6.5 days. This is projected to increase by between 1.1 and 1.8 days under RCP 8.5 by the 2050s. These changes are relatively uniform across the state.

A major benefit of this approach is that it can be updated quickly using new climate model projections. Rather than having to run all precipitation and temperature statistics on new downscaled climate model projections, all that is required is the annual and seasonal temperature increases from those projections for particular target years. Those temperature increases can then be mapped directly to the appropriate weather generator scenario, and delta changes in precipitation and temperature statistics (which are already archived from the weather generator simulations) can be immediately updated in the above tables and corresponding spatial maps.

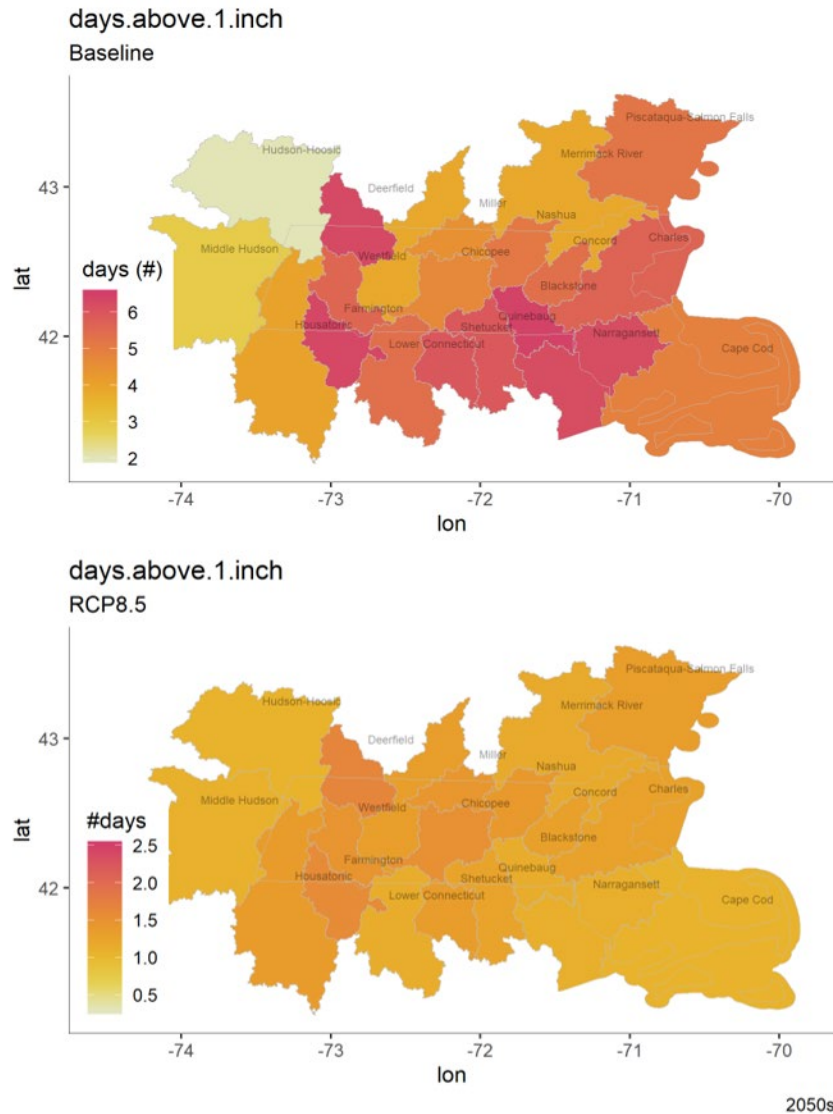


Figure 12. Projected change in the number of days with greater than 1 inch of precipitation for the full year and all 20 HUC8 watersheds in Massachusetts for the 2050s projection horizon. The Baseline (top row) shows the average number of days per year with greater than 1 inch of precipitation in baseline runs of the weather generator (i.e., no thermodynamic climate change). The bottom row shows the change in the number of days over the baseline, based on weather generator simulations with median temperature increases associated with the RCP 8.5 scenario. A darker shade of color indicates more number of days - as an absolute value for the Baseline- and changes in the number of days for the projected scenario.

5. Summary

This report presents the development of a stochastic weather generator for the creation of climate change scenarios across the state of Massachusetts. The stochastic weather generator is novel in comparison with other downscaling techniques, because it is designed to distinguish thermodynamic and dynamic mechanisms of climate change, and propagate only those mechanisms deemed credible for planning purposes. In this work, the weather generator was calibrated across 20 different HUC8 watersheds that intersect with the state of Massachusetts based on a subset of performance metrics, and then was validated using a more comprehensive set of performance metrics for those same basins. After calibrating and validating the model, the stochastic weather generator was used to create a large ensemble of future climate scenarios that reflect thermodynamic climate changes only, mainly temperature increases and the direct scaling of extreme precipitation with temperature. Using this ensemble, delta changes were calculated for a set of precipitation and temperature statistics for each of the HUC8 basins, which will ultimately be reported on the Resilient MA website to support local and statewide decision-making with regard to climate change adaptation across Massachusetts.

Acknowledgements

This work was supported by the Massachusetts Executive Office of Energy and Environmental Affairs.

References

- Abatzoglou, J. T. (2013). Development of gridded surface meteorological data for ecological applications and modelling. *Int. J. Climatol.*, 33, 121–131.
- Abatzoglou, J.T., and Brown, T.J. (2012). A comparison of statistical downscaling methods suited for wildfire applications. *International Journal of Climatology*, 32, 772-780.
- Alduchov, O. A., & Eskridge, R. E. (1996). Improved Magnus form approximation of saturation vapor pressure. *Journal of applied meteorology*, 35(4), 601–609.
- Allen, M. R., and Ingram, W.J. (2002), Constraints on future changes in climate and the hydrologic cycle. *Nature*, 419, 224–232, doi:10.1038/nature01092.
- Bao, J., Sherwood, S.C., Alexander, L.V., and Evans, J.P. (2017), Future increases in extreme precipitation exceed observed scaling rates, *Nature Climate Change*, 7, 128-133, DOI: 10.1038/NCLIMATE3201.
- Baum, L. E., & Petrie, T. (1966), Statistical inference for probabilistic functions of finite state Markov chains. *The annals of mathematical statistics*, 37(6), 1554-1563.
- Baum, L. E., and T. Petrie, G. Soules, and N. Weiss, (1970), A Maximization Technique Occurring in the Statistical Analysis of Probabilistic Functions of Markov Chains. *Ann. Math. Stat.*, 41, 164–171, <https://doi.org/10.1214/aoms/1177697196>.
- Brekke, L. D., E. P. Maurer, J. D. Anderson, M. D. Dettinger, E. S. Townsley, A. Harrison, and T. Pruitt (2009), Assessing reservoir operations risk under climate change, *Water Resour. Res.*, 45, W04411, doi:10.1029/2008WR006941.
- Dai, A. (2011), Drought under global warming: a review, *WIREs: Climate Change*, 2(1), 45-65.
- Daly, C., R. P. Neilson, and Phillips, D.L. (1994), A statistical topographic model for mapping climatological precipitation over mountainous terrain, *J. Appl. Meteor.*, 33, 140–158.

- Dempster, A. P., N. M. Laird, and D. B. Rubin, 1977: Maximum Likelihood from Incomplete Data Via the EM Algorithm . *J. R. Stat. Soc. Ser. B*, 39, 1–22, <https://doi.org/10.1111/j.2517-6161.1977.tb01600.x>.
- Emori, S., and Brown, S.J. (2005), Dynamic and thermodynamic changes in mean and extreme precipitation under climate change, *Geophysical Research Letters*, 32 (17), L17706, doi:10.1029/2005GL023272.
- Fischer, E.M., and Knutti, R. (2016), Observed heavy precipitation increase confirms theory and early models, *Nat. Clim. Change*, 6 (11), 986–991. <http://dx.doi.org/10.1038/nclimate3110>.
- Forney, G. D. (1973). The viterbi algorithm. *Proceedings of the IEEE*, 61(3), 268-278.
- Fowler, H.J., Blenkinsop, S., and Tebaldi, C. (2007), Review: Linking climate change modeling to impact studies: recent advances in downscaling techniques for hydrologic modeling, *International Journal of Climatology*, 27, 1547-1578.
- Guerreiro, S.B., Fowler, H.J., Barbero, R., Westra, S. Lenderink, G., Blenkinsop, S., Lewis, E., and Li, X.-F. (2018), Detection of continental-scale intensification of hourly rainfall extremes, *Nature Climate Change*, 8, 803-807, <https://doi.org/10.1038/s41558-018-0245-3>.
- Gupta, H. V., Sorooshian, S., & Yapo, P. O. (1998). Toward improved calibration of hydrologic models: Multiple and noncommensurable measures of information. *Water Resources Research*, 34(4), 751-763.
- Hawcroft, M., Walsh, E., Hodges, K.I., and Zappa, G. (2018), Significantly increased extreme precipitation expected in Europe and North America from extratropical cyclones, *Environmental Research Letters*, <https://doi.org/10.1088/1748-9326/aaed59>.
- Hughes, J. P., and Guttorp, P. (1994). A class of stochastic models for relating synoptic atmospheric patterns to regional hydrologic phenomena. *Water resources research*, 30(5), 1535-1546.
- Hughes, J. P., Guttorp, P., & Charles, S. P. (1999). A non-homogeneous hidden Markov model for precipitation occurrence. *Journal of the Royal Statistical Society: Series C (Applied Statistics)*, 48(1), 15-30.
- IPCC (2013), *Climate Change 2013: The Physical Science Basis. Contribution of Working Group I to the Fifth Assessment Report of the Intergovernmental Panel on Climate Change* [Stocker, T.F., D. Qin, G.-K. Plattner, M. Tignor, S.K. Allen, J. Boschung, A. Nauels, Y. Xia, V. Bex and P.M. Midgley (eds.)]. Cambridge University Press, Cambridge, United Kingdom and New York, NY, USA, 1535 pp.
- Jiménez Cisneros, B.E., T. Oki, N.W. Arnell, G. Benito, J.G. Cogley, P. Döll, T. Jiang, and S.S. Mwakalila (2014), Freshwater resources. In: *Climate Change 2014: Impacts, Adaptation, and Vulnerability. Part A: Global and Sectoral Aspects. Contribution of Working Group II to the Fifth Assessment Report of the Intergovernmental Panel on Climate Change* [Field, C.B., V.R. Barros, D.J. Dokken, K.J. Mach, M.D. Mastrandrea, T.E. Bilir, M. Chatterjee, K.L. Ebi, Y.O. Estrada, R.C. Genova, B. Girma, E.S. Kissel, A.N. Levy, S. MacCracken, P.R. Mastrandrea, and L.L. White (eds.)]. Cambridge University Press, Cambridge, United Kingdom and New York, NY, USA, pp. 229-269.
- Jones, C., Giorgi, F., and Asrar, G. (2011). The Coordinated Regional Downscaling Experiment: CORDEX; an international downscaling link to CMIP5. *CLIVAR Exch.*, 16, 34–40.
- Kendon, E.J., N. Ban, N.M. Roberts, H.J. Fowler, M.J. Roberts, S.C. Chan, J.P. Evans, G. Fosser, and J.M. Wilkinson, 2017: Do Convection-Permitting Regional Climate Models

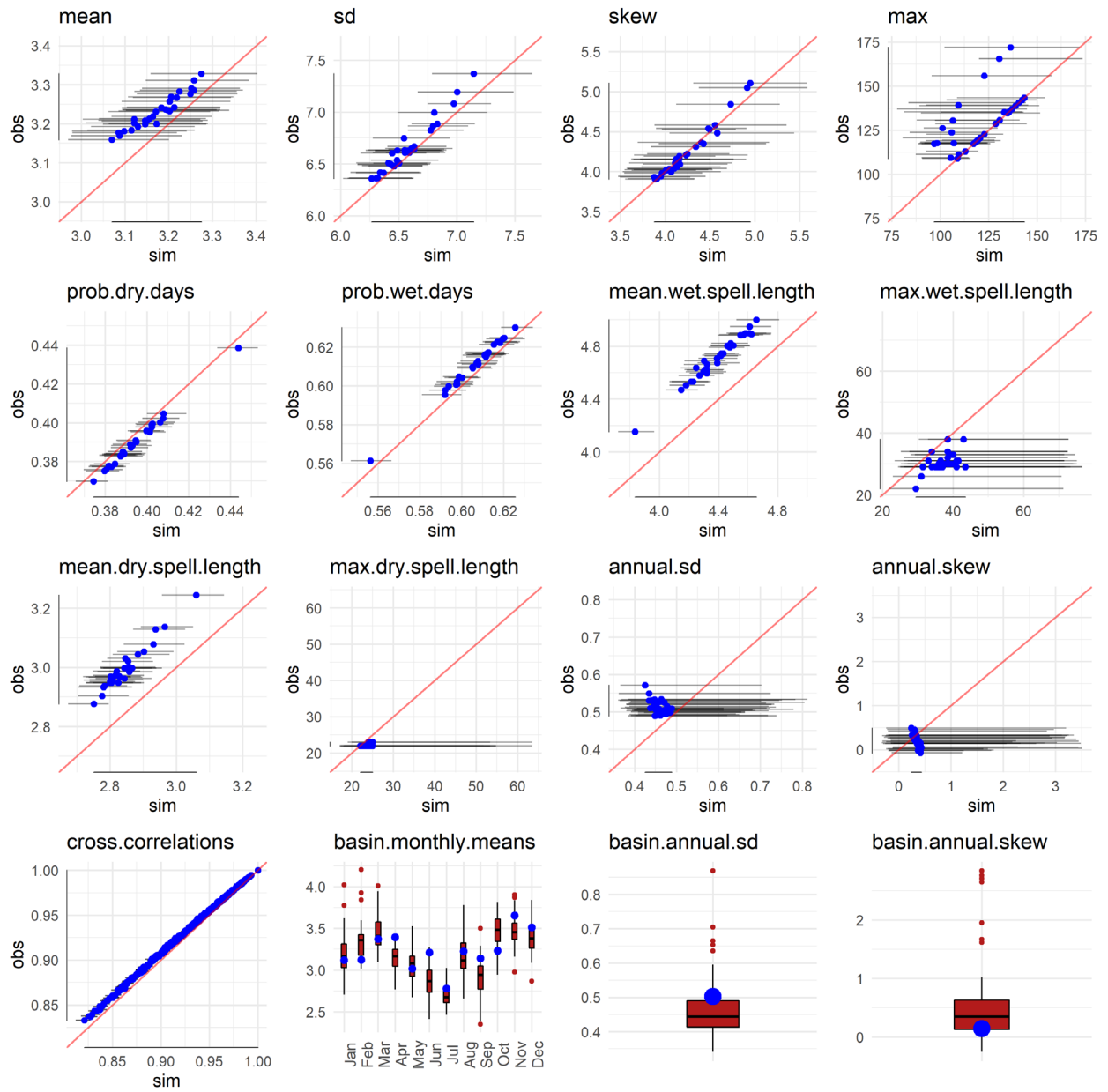
- Improve Projections of Future Precipitation Change?. *Bull. Amer. Meteor. Soc.*, 98, 79–93, <https://doi.org/10.1175/BAMS-D-15-0004.1>
- Kysely, J., Z. Rulfova, A. Farda, and M. Hanel (2015), Convective and stratiform precipitation characteristics in an ensemble of regional climate model simulations, *Climate Dynamics*, 1-17, doi: 10.1007/s00382-015-2580-7.
- Lenderink, G., R. Barbero, J.M. Loriaux, and H.J. Fowler (2017), Super-Clausius–Clapeyron Scaling of Extreme Hourly Convective Precipitation and Its Relation to Large-Scale Atmospheric Conditions, *J. Climate*, 30, 6037–6052, <https://doi.org/10.1175/JCLI-D-16-0808.1>
- Li, G., S. P. Harrison, P. J. Bartlein, K. Izumi, and I. Colin Prentice (2013), Precipitation scaling with temperature in warm and cold climates: An analysis of CMIP5 simulations, *Geophys. Res. Lett.*, 40, 4018–4024, doi: 10.1002/grl.50730.
- Livneh B., T.J. Bohn, D.S. Pierce, F. Munoz-Ariola, B. Nijssen, R. Vose, D. Cayan, and L.D. Brekke, 2015: A spatially comprehensive, hydrometeorological data set for Mexico, the U.S., and southern Canada 1950-2013, *Nature Scientific Data*, 5:150042, doi:10.1038/sdata.2015.42.
- Lu, J., L. Ruby Leung, Q. Yang, G. Chen, W. D. Collins, F. Li, Z. Jason Hou, and X. Feng (2014), The robust dynamical contribution to precipitation extremes in idealized warming simulations across model resolutions, *Geophys. Res. Lett.*, 41, 2971–2978, doi:10.1002/2014GL059532.
- Maher, P., Vallis, G. K., Sherwood, S. C., Webb, M. J., & Sansom, P.G. (2018). The impact of parameterized convection on climatological precipitation in atmospheric global climate models. *Geophysical Research Letters*, 45, 3728–3736. <https://doi.org/10.1002/2017GL076826>
- Maraun, D., et al. (2017), Towards process-informed bias correction of climate change simulations. *Nat. Climate Change*, 7, 764–773, <https://doi.org/10.1038/nclimate3418>.
- Muller, C.J., and O’Gorman, P.A. (2011), An energetic perspective on the regional response of precipitation to climate change, *Nature Climate Change*, 1 (5), 266-271.
- Muñoz, Á.G., X. Yang, G.A. Vecchi, A.W. Robertson, and W.F. Cooke, 2017: A Weather-Type-Based Cross-Time-Scale Diagnostic Framework for Coupled Circulation Models. *J. Climate*, 30, 8951–8972, <https://doi.org/10.1175/JCLI-D-17-0115.1>
- Najibi, N., Mukhopadhyay, S., Steinschneider, S. (2021), Identifying weather regimes for regional-scale stochastic weather generators, *International Journal of Climatology*, 41, 2456–2479. <https://doi.org/10.1002/joc.6969>.
- O’Gorman, P.A. (2015), Precipitation extremes under climate change, *Curr. Clim. Change Rep.*, 49-59, doi: 10.1007/s40641-015-0009-3.
- Pendergrass, A.G., and Hartmann, D.L. (2014a), Two modes of change of the distribution of rain, *Journal of Climate*, 27(22), 8357-8371.
- Pendergrass, A.G., and Hartmann, D.L. (2014b), The atmospheric energy constraint on global-mean precipitation change, *Journal of Climate*, 27(2), 757-768.
- Pfahl S., O’Gorman, P.A., Fischer, E.M. (2017), Understanding the regional pattern of projected future changes in extreme precipitation, *Nature Climate Change*, 7 (6), 423-427.
- Rabiner, L. R., 1989: A tutorial on hidden Markov models and selected applications in speech recognition. *Proc. IEEE*, 77, 257--286.
- Richardson, C. W. (1981), Stochastic simulation of daily precipitation, temperature, and solar radiation, *Water Resour. Res.*, 17(1), 182–190, doi: 10.1029/WR017i001p00182.

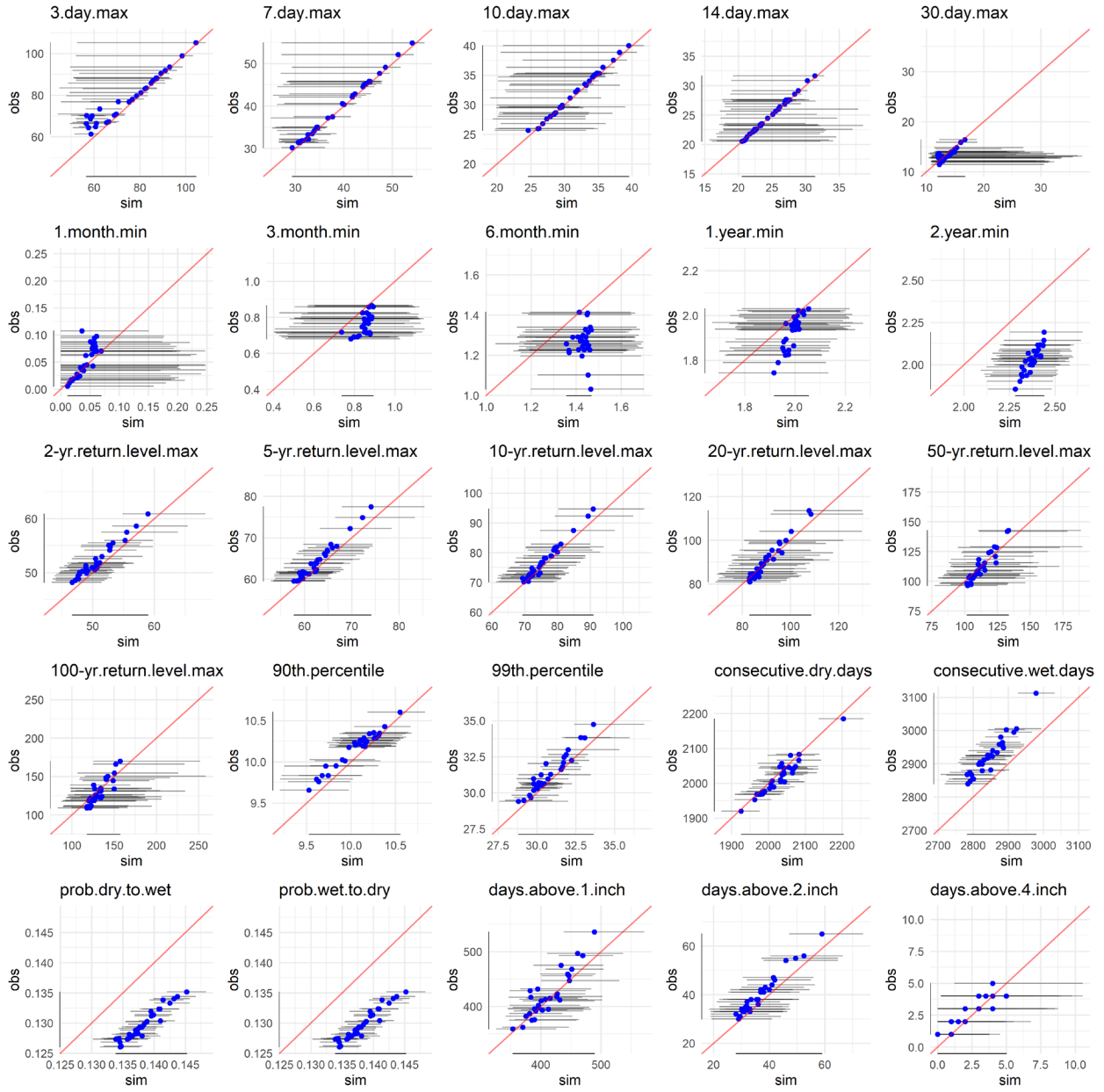
- Robertson, A.W., and Ghil, M. (1999), Large-scale weather regimes and local climate over the western United States, *Journal of Climate*, 12, 1796-1813.
- Robertson, A.W., Y. Kushnir, U. Lall, and J. Nakamura (2015), Weather and climatic drivers of extreme flooding events over the Midwest of the United States. *Extreme Events: Observations, Modeling, and Economics*, Geophys.Monogr., Vol. 214, Amer.Geophys. Union, 113–124.
- Seager, R., Naik, N., and Vecchi, G.A. (2010), Thermodynamic and dynamic mechanisms for large-scale changes in the hydrologic cycle in response to global warming, *Journal of Climate*, 23 (17), 4651-4668.
- Seager, R., Neelin, D., Simpson, I., Liu, H., Henderson, N., Shaw, T., Kushnir, Y., and Ting, M. (2014), Dynamical and Thermodynamical Causes of Large-Scale Changes in the Hydrological Cycle over North America in Response to Global Warming, *Journal of Climate*, 27 (20), 7921-7948.
- Shepard, D. S., (1984), Computer mapping: The SYMAP interpolation algorithm, *Spatial Statistics and Models*, G. L. Gaile and C. J. Willmott, Eds., D. Reidel, 133–145.
- Shepherd, T.G. (2014), Atmospheric circulation as a source of uncertainty in climate change projections, *Nature Geosciences*, 7, 703-708, doi:10.1038/ngeo2253.
- Steinschneider, S., Ray, P., Rahat, S.H., and Kucharski, J. (2019), A weather-regime based stochastic weather generator for climate vulnerability assessments of water systems in the Western United States, *Water Resources Research*, 55. <https://doi.org/10.1029/2018WR024446>.
- Stephens, G. L., T. L'Ecuyer, R. Forbes, A. Gettleman, J.-C. Golaz, A. Bodas-Salcedo, K. Suzuki, P. Gabriel, and J. Haynes (2010), Dreary state of precipitation in global models, *J. Geophys. Res.*, 115, D24211, doi:10.1029/2010JD014532.
- Stephenson, D. B., Collins, M., Rougier, J. C., and Chandler, R. E. (2012), Statistical problems in the probabilistic prediction of climate change, *Environmetrics*, 23(5), 364–372.
- Tan, J., Oreopoulos, L., Jakob, C., and Jin, D. (2018), Evaluating rainfall errors in global climate models through cloud regimes, *Climate Dynamics*, 50 (9-10), 3301-3314.
- Taylor, K.E., Stouffer, R.J., Meehl, G.A., (2012), An overview of CMIP5 and the experiment design. *Bull. Am. Meteorol. Soc.* 93 (4), 485–498.
- Ting, M., Seager, R., Li, C., Liu, H., and Henderson, N. (2018), Mechanism of future spring drying in the southwestern United States in CMIP5 models, *Journal of Climate*, 31 (11), 4265-4279.
- Trenberth, K. E. (2011), Changes in precipitation with climate change, *Climate Research*, 47, 123-138, doi: 10.3354/cr00953.
- Trenberth, K.E., Dai, A., van der Schrier, G., Jones, P.D., Barichivich, J., Briffa, K.R., and Sheffield, J. (2013), Global warming and changes in drought, *Nature Climate Change*, 4, doi: 10.1038/NCLIMATE2067.
- Visser, I., and M. Speekenbrink, 2010: depmixS4: An R package for hidden markov models. *J. Stat. Softw.*, 36, 1–21, <https://doi.org/10.18637/jss.v036.i07>.
- Westra, S., H. J. Fowler, J.P., Evans, L. V. Alexander, P. Berg, F. Johnson, E. J. Kendon, G. Lenderink, and N. M. Roberts (2014), Future changes to the intensity and frequency of short- duration extreme rainfall, *Rev. Geophys.*, 52,522–555, doi:10.1002/2014RG000464.
- Wilks D.S. (2010), Use of stochastic weather generators for precipitation downscaling, *WIRES Clim Change* 2010, 1(6), 898–907
- Wilks, D. S. (2002), Realizations of daily weather in forecast seasonal climate, J.

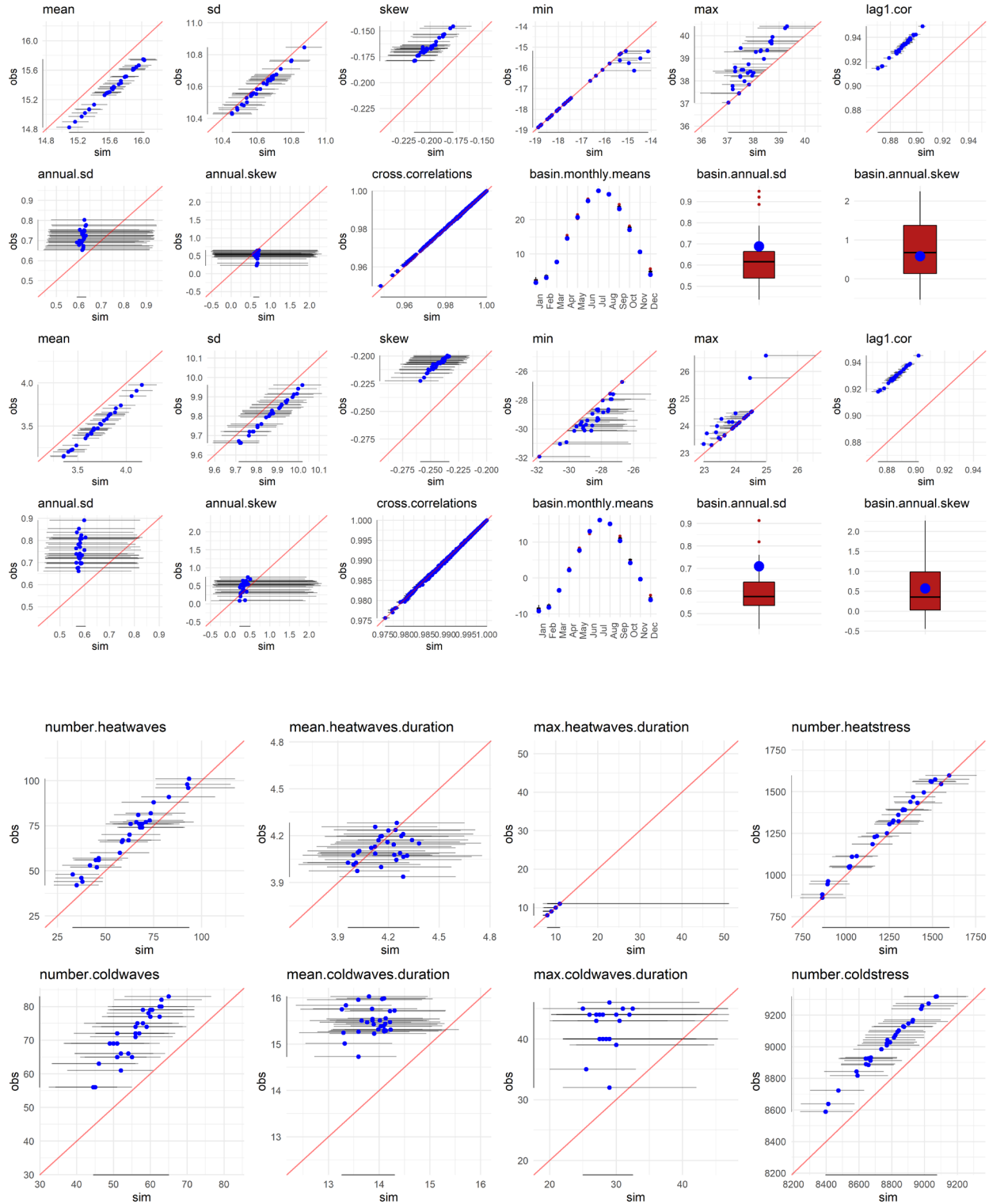
- Hydrometeorol., 3, 195–207.
- Wilks, D. S., and R. L. Wilby (1999), The weather generation game: A review of stochastic weather models, *Prog. Phys. Geogr.*, 23, 329–357.
- Wilks, D.S. (2012), Stochastic weather generators for climate-change downscaling, part II: multivariate and spatially coherent multisite downscaling, *WIREs: Climate Change*, 3(3), 267-278.
- Woollings, T. (2010), Dynamical influences on European climate: an uncertain future. *Phil. Trans. R. Soc. A* 368, 3733–3756.
- Zappa, G., Shaffrey, L. C. & Hodges, K. I. (2013), The ability of CMIP5 models to simulate North Atlantic extratropical cyclones. *J. Clim.* 26, 5379–5396.

Appendix

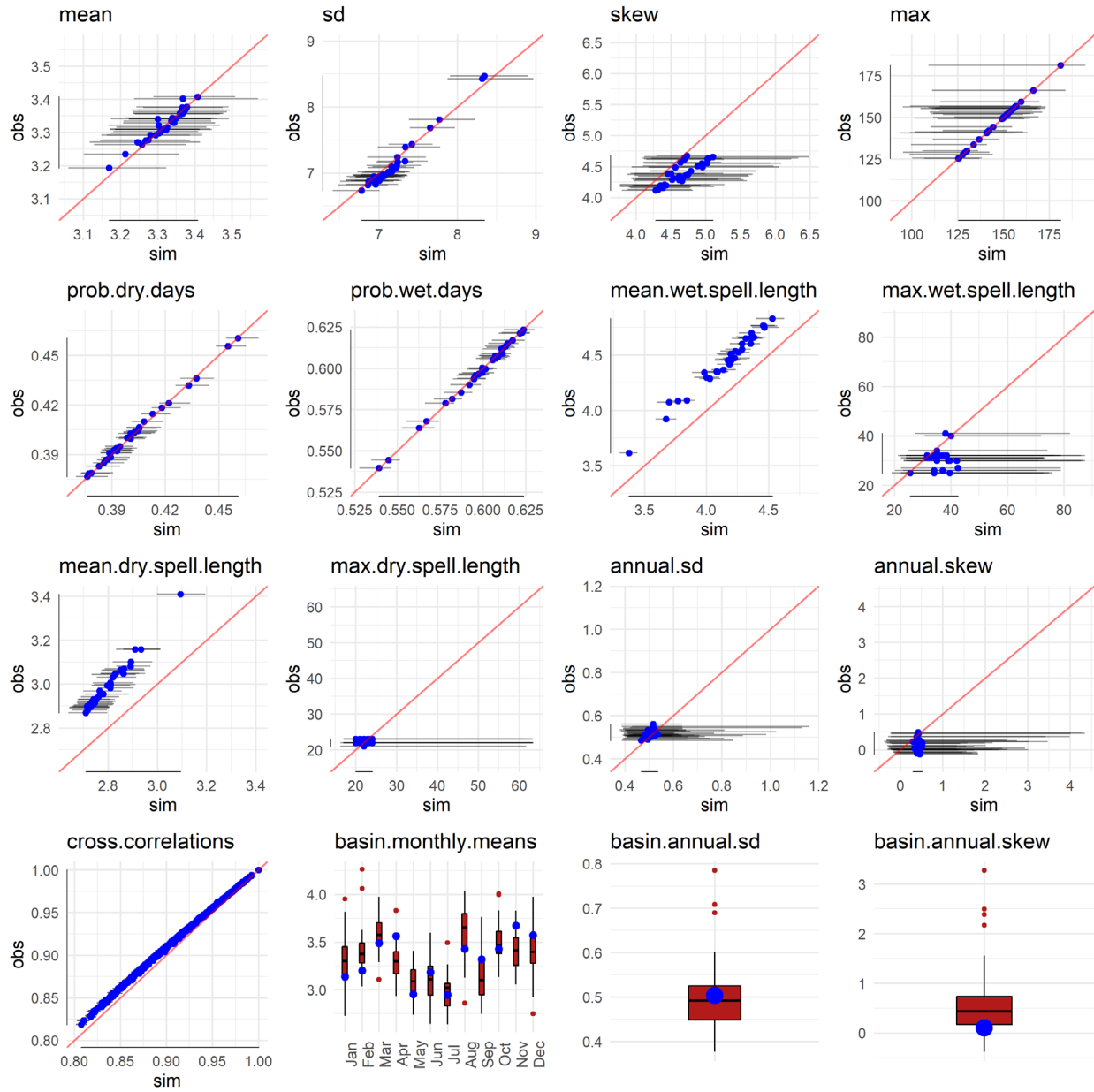
Concord

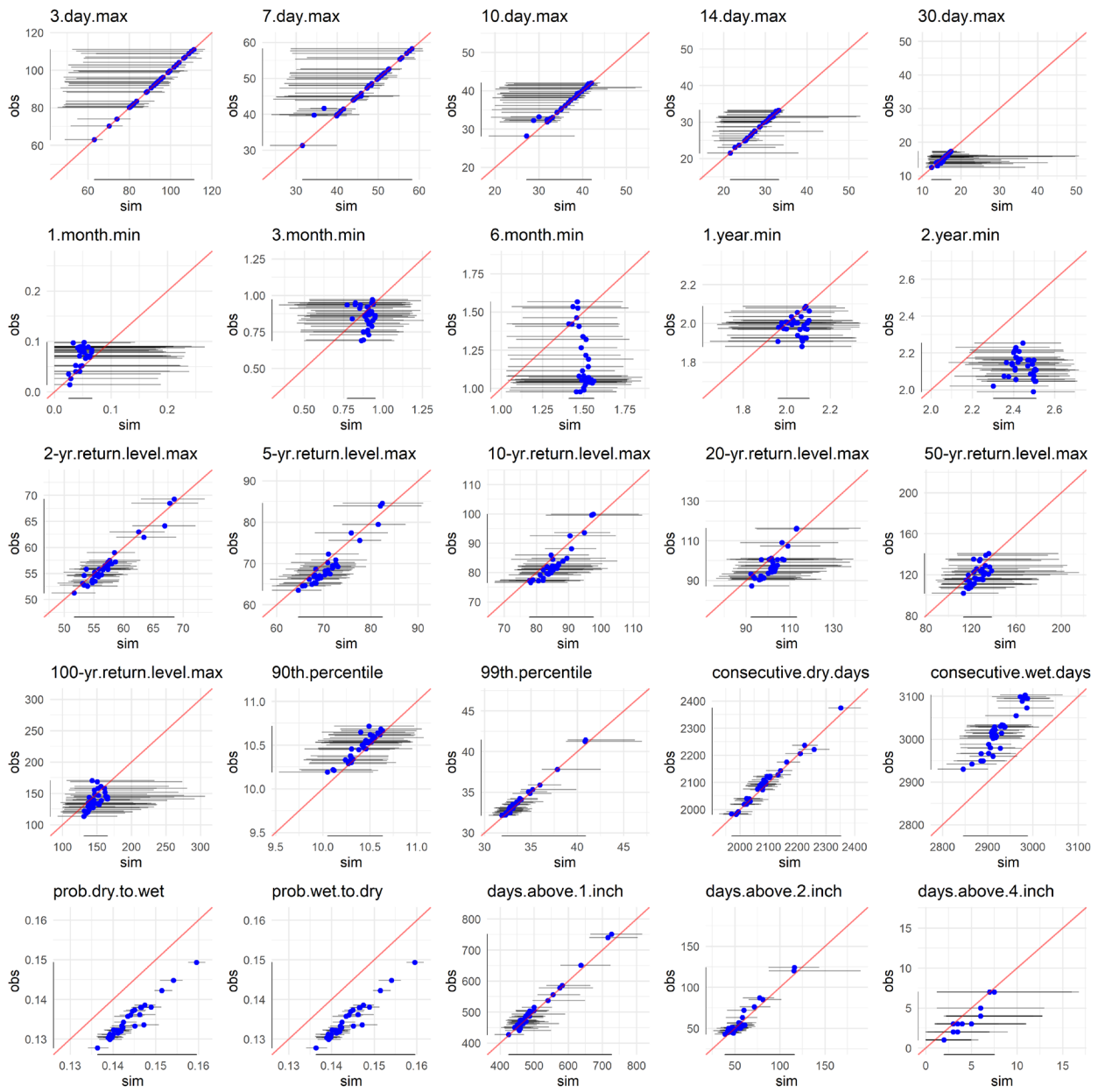


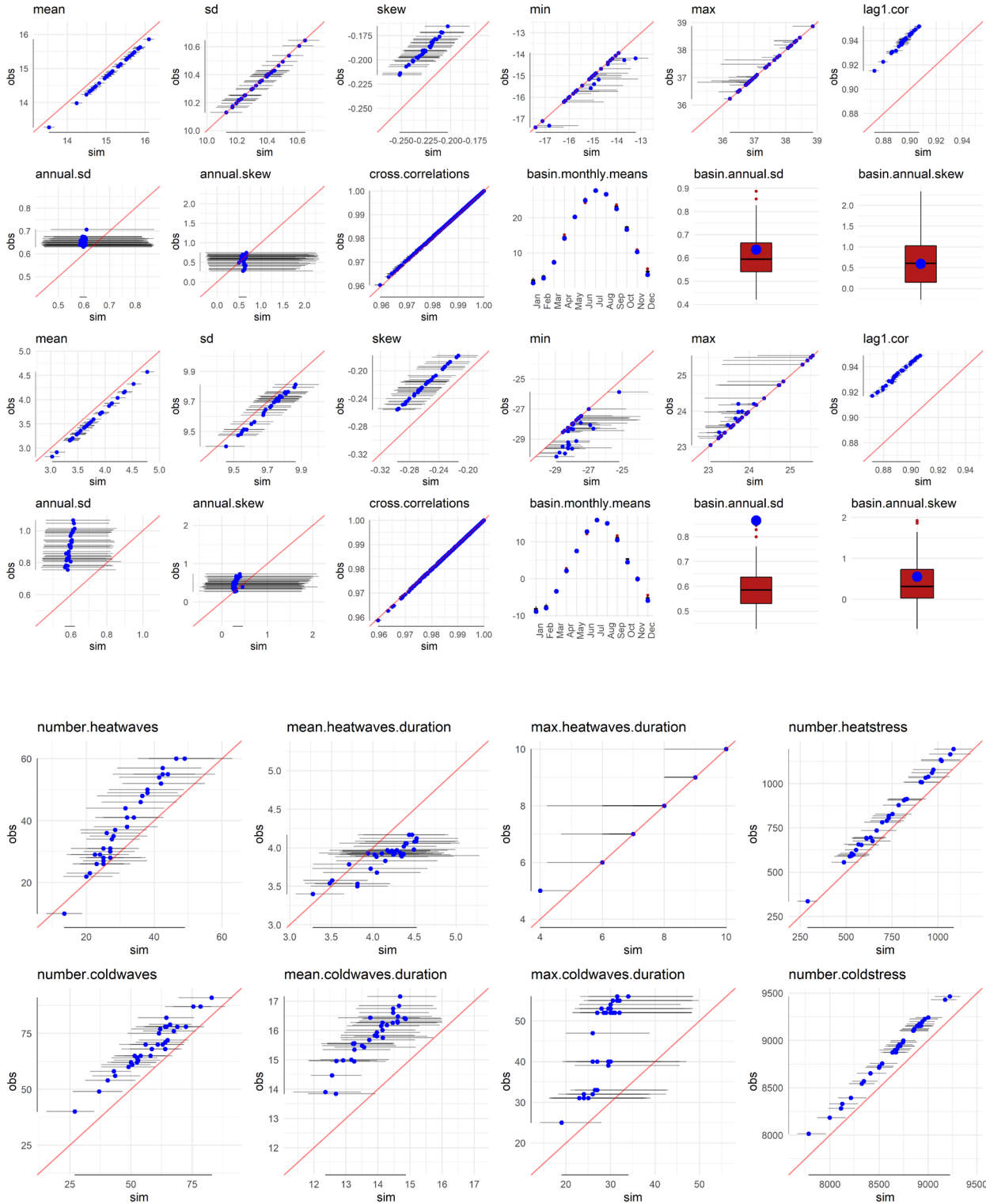




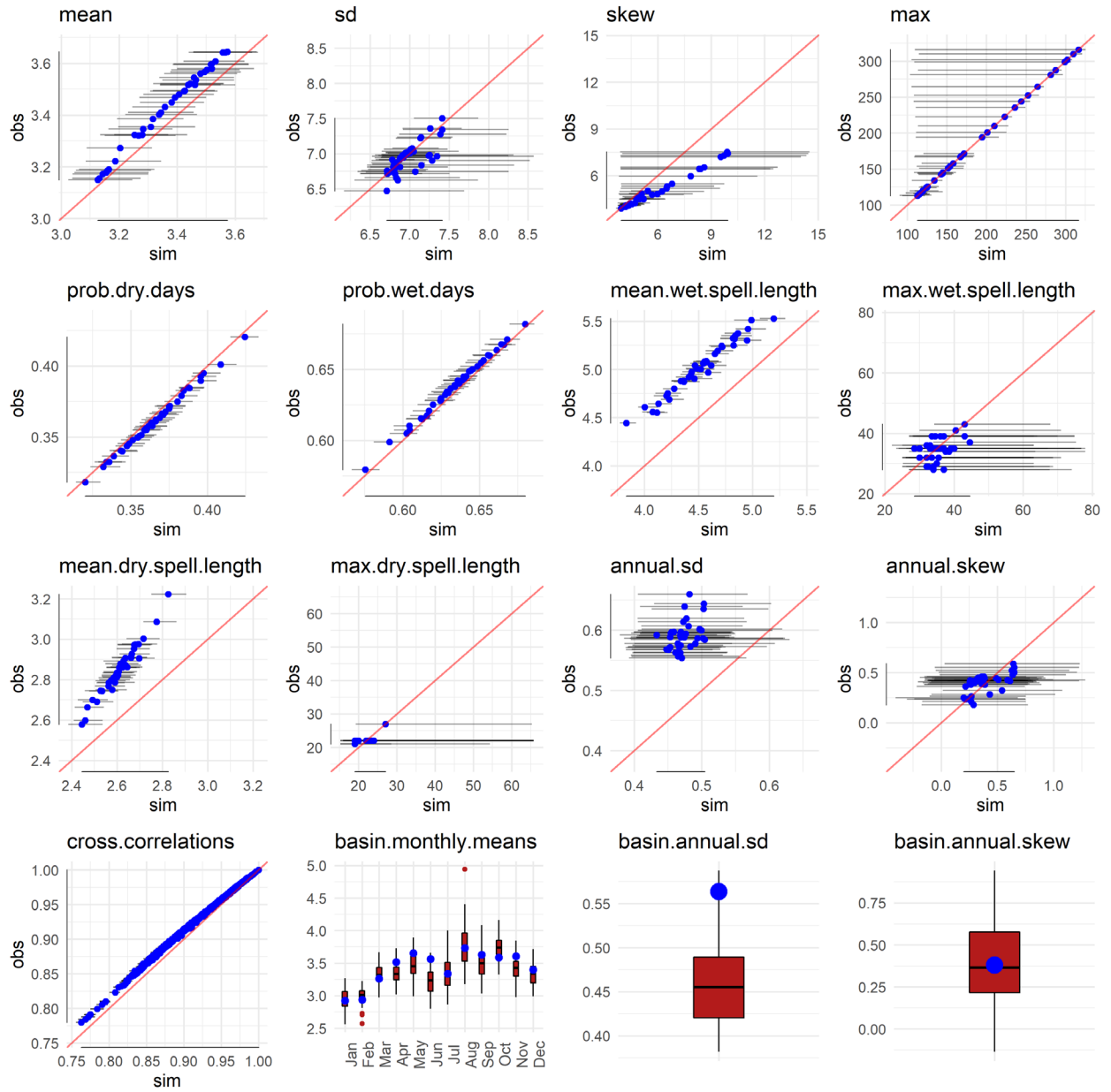
Blackstone

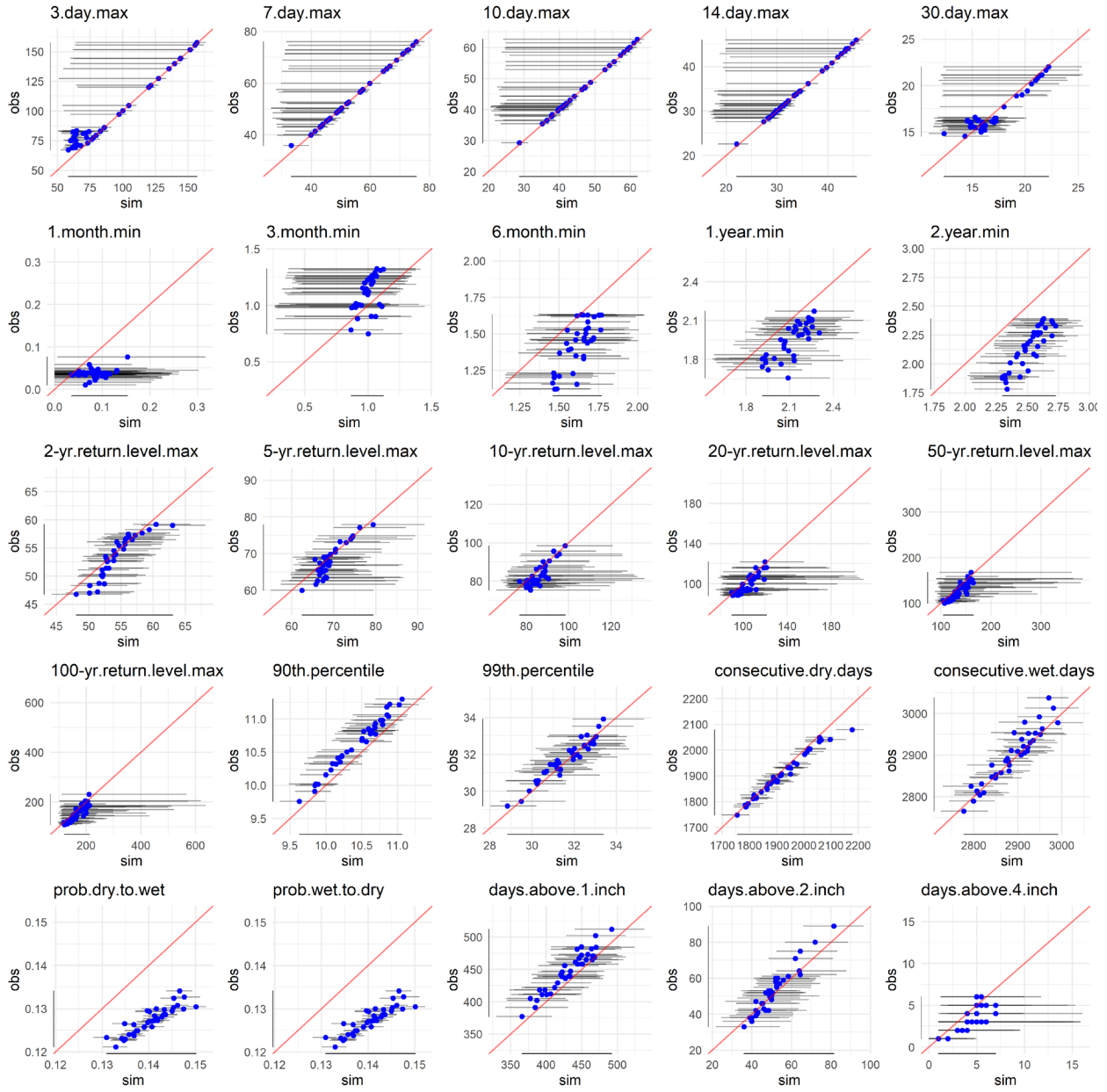


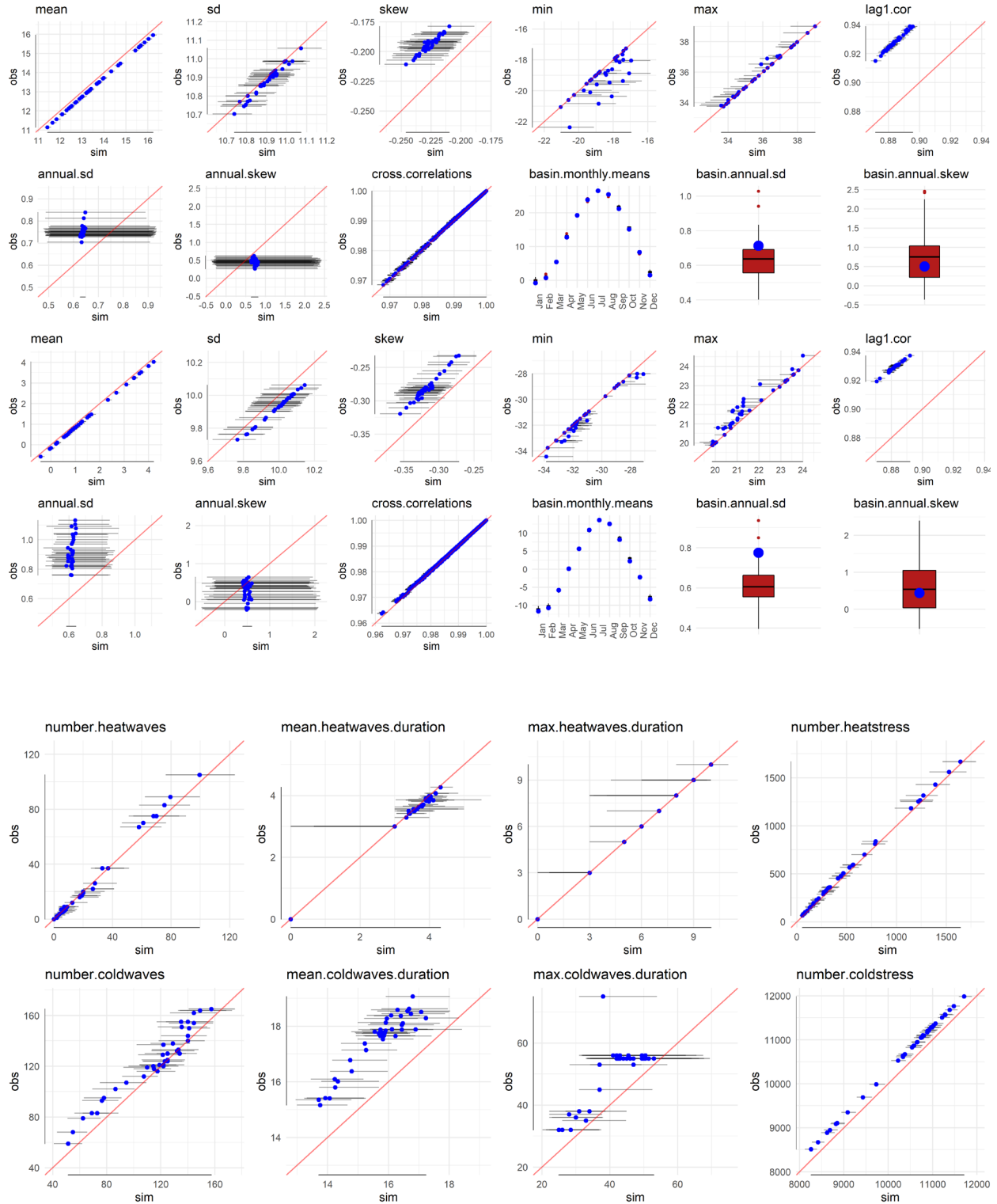




Westfield







Temperature Changes by Season from MACA

Table S1. Same as Table 6, but for winter (DJF).

RCP 8.5												
DJF	2030s			2050s			2070s			2090s		
basin no.	10th	50th	90th									
1	1.41	2.27	3.22	2.51	3.56	4.84	3.65	5.06	6.80	4.30	6.10	7.76
2	1.50	2.30	3.31	2.50	3.64	4.99	3.66	5.16	6.90	4.27	6.19	7.95
3	1.31	2.03	2.84	2.26	3.17	4.27	3.20	4.49	5.79	3.82	5.40	6.79
4	1.37	2.13	2.99	2.38	3.31	4.50	3.34	4.69	6.22	3.97	5.65	7.20
5	1.45	2.21	3.09	2.44	3.44	4.69	3.49	4.86	6.45	4.19	5.83	7.45
6	1.37	2.09	2.93	2.33	3.31	4.47	3.39	4.69	6.12	4.06	5.64	7.10
7	1.42	2.13	2.98	2.38	3.34	4.53	3.39	4.72	6.16	4.07	5.65	7.13
8	1.47	2.25	3.20	2.48	3.56	4.85	3.61	5.07	6.69	4.32	6.10	7.73
9	1.40	2.12	2.97	2.37	3.33	4.49	3.41	4.72	6.17	4.11	5.67	7.16
10	1.42	2.19	3.10	2.42	3.43	4.69	3.46	4.85	6.44	4.12	5.82	7.44
11	1.43	2.23	3.13	2.48	3.49	4.72	3.62	4.95	6.60	4.27	5.95	7.59
12	1.37	2.15	3.00	2.40	3.38	4.57	3.48	4.80	6.38	4.15	5.78	7.36
13	1.43	2.25	3.21	2.49	3.58	4.84	3.67	5.09	6.73	4.38	6.13	7.75
14	1.47	2.21	3.13	2.45	3.47	4.70	3.54	4.91	6.52	4.23	5.90	7.49
15	1.23	1.99	2.78	2.17	3.09	4.13	2.99	4.35	5.61	3.61	5.23	6.58
16	1.39	2.27	3.23	2.48	3.56	4.82	3.66	5.06	6.71	4.32	6.09	7.69
17	1.47	2.29	3.25	2.51	3.65	4.91	3.70	5.18	6.83	4.42	6.23	7.90
18	1.53	2.41	3.49	2.60	3.81	5.14	3.79	5.39	7.16	4.51	6.47	8.34
19	1.41	2.13	2.98	2.39	3.32	4.50	3.40	4.69	6.16	4.08	5.63	7.13
20	1.49	2.31	3.27	2.52	3.67	4.94	3.70	5.23	6.90	4.40	6.30	8.03

Table S2. Same as Table 6, but for spring (MAM).

RCP 8.5												
MAM	2030s			2050s			2070s			2090s		
basin no.	10th	50th	90th									
1	0.84	1.79	3.07	1.91	3.05	4.72	2.94	4.31	6.29	3.77	5.33	7.61
2	0.94	1.80	3.12	1.94	3.05	4.47	2.88	4.25	5.90	3.50	5.25	7.25
3	0.82	1.67	2.84	1.74	2.84	4.30	2.61	3.98	5.78	3.55	4.91	6.71
4	0.83	1.73	2.96	1.81	2.94	4.48	2.72	4.11	5.99	3.61	5.09	7.09
5	0.94	1.75	3.03	1.89	2.96	4.39	2.74	4.11	5.76	3.50	5.07	7.06
6	0.83	1.66	2.90	1.81	2.88	4.37	2.64	4.04	5.81	3.54	5.00	6.94
7	0.88	1.68	2.95	1.83	2.88	4.38	2.64	4.00	5.74	3.52	4.93	6.81
8	0.94	1.77	3.07	1.93	3.02	4.43	2.81	4.21	5.91	3.54	5.21	7.28
9	0.85	1.69	2.93	1.81	2.89	4.41	2.65	4.05	5.88	3.54	5.01	6.98
10	0.94	1.74	3.02	1.89	2.96	4.38	2.76	4.11	5.76	3.50	5.08	7.05
11	0.89	1.77	3.07	1.88	3.00	4.49	2.79	4.19	5.97	3.60	5.18	7.35
12	0.84	1.72	2.99	1.83	2.95	4.48	2.70	4.14	5.97	3.59	5.12	7.18
13	0.90	1.76	3.07	1.90	3.03	4.46	2.86	4.26	6.00	3.64	5.27	7.42
14	0.92	1.74	3.05	1.86	2.97	4.43	2.75	4.16	5.91	3.56	5.14	7.26
15	0.77	1.67	2.73	1.70	2.80	4.17	2.56	3.89	5.60	3.42	4.77	6.63
16	0.89	1.79	3.10	1.91	3.04	4.59	2.89	4.27	6.10	3.68	5.27	7.50
17	0.93	1.78	3.10	1.94	3.04	4.47	2.86	4.27	5.99	3.61	5.28	7.41
18	1.00	1.87	3.26	1.98	3.12	4.62	2.93	4.34	6.09	3.62	5.35	7.49
19	0.86	1.71	2.95	1.81	2.91	4.43	2.65	4.06	5.89	3.54	5.01	6.97
20	0.92	1.79	3.10	1.94	3.06	4.46	2.86	4.30	5.99	3.58	5.33	7.43

Table S3. Same as Table 6, but for summer (JJA).

RCP 8.5												
JJA	2030s			2050s			2070s			2090s		
basin no.	10th	50th	90th									
1	1.24	2.02	2.79	2.22	3.37	4.55	3.22	4.79	6.55	3.94	5.88	8.02
2	1.28	2.09	2.66	2.27	3.43	4.46	3.24	4.87	6.25	4.01	5.98	7.57
3	1.22	1.87	2.59	2.25	3.15	4.23	3.16	4.42	5.75	3.92	5.38	6.87
4	1.28	1.94	2.66	2.25	3.25	4.40	3.16	4.58	6.13	3.94	5.60	7.35
5	1.37	2.05	2.65	2.31	3.35	4.34	3.19	4.68	5.93	3.90	5.71	7.04
6	1.31	1.92	2.54	2.32	3.25	4.24	3.24	4.59	5.81	3.98	5.61	6.98
7	1.35	1.94	2.56	2.34	3.22	4.19	3.21	4.51	5.68	3.94	5.49	6.81
8	1.30	2.04	2.66	2.28	3.40	4.45	3.23	4.81	6.15	3.95	5.90	7.42
9	1.31	1.95	2.59	2.29	3.25	4.28	3.19	4.57	5.85	3.90	5.57	6.99
10	1.33	2.04	2.63	2.29	3.35	4.32	3.19	4.70	5.95	3.93	5.75	7.10
11	1.30	2.02	2.72	2.25	3.35	4.46	3.19	4.72	6.27	3.88	5.78	7.57
12	1.29	1.96	2.67	2.26	3.29	4.41	3.20	4.64	6.16	3.93	5.68	7.36
13	1.26	2.01	2.69	2.25	3.39	4.52	3.24	4.84	6.37	3.97	5.94	7.76
14	1.29	2.01	2.67	2.27	3.35	4.43	3.22	4.72	6.12	3.90	5.78	7.34
15	1.10	1.83	2.60	2.19	3.06	4.14	3.11	4.28	5.59	3.89	5.18	6.64
16	1.26	2.03	2.76	2.23	3.38	4.51	3.21	4.80	6.46	3.92	5.88	7.92
17	1.27	2.03	2.68	2.25	3.40	4.51	3.23	4.84	6.34	3.95	5.95	7.73
18	1.31	2.13	2.74	2.26	3.47	4.55	3.25	4.91	6.48	3.97	6.03	7.94
19	1.32	1.96	2.63	2.28	3.25	4.31	3.17	4.55	5.90	3.89	5.55	7.02
20	1.26	2.04	2.68	2.25	3.43	4.54	3.25	4.90	6.42	3.96	6.02	7.84

Table S4. Same as Table 6, but for fall (SON).

RCP 8.5												
SON	2030s			2050s			2070s			2090s		
basin no.	10th	50th	90th									
1	1.33	2.06	2.89	2.29	3.28	4.22	3.49	4.73	5.96	4.40	5.78	7.35
2	1.35	2.14	2.91	2.29	3.36	4.23	3.53	4.84	6.01	4.47	5.90	7.56
3	1.29	1.98	2.78	2.23	3.11	4.01	3.38	4.44	5.60	4.23	5.40	7.03
4	1.32	2.03	2.81	2.27	3.19	4.09	3.47	4.56	5.72	4.31	5.55	7.15
5	1.39	2.10	2.85	2.30	3.27	4.14	3.50	4.67	5.80	4.43	5.69	7.27
6	1.28	2.00	2.80	2.23	3.18	4.07	3.48	4.59	5.71	4.41	5.60	7.22
7	1.34	2.05	2.84	2.26	3.20	4.07	3.45	4.56	5.69	4.37	5.55	7.16
8	1.37	2.09	2.86	2.31	3.31	4.18	3.54	4.78	5.92	4.49	5.84	7.46
9	1.32	2.02	2.85	2.22	3.19	4.08	3.47	4.58	5.69	4.38	5.57	7.18
10	1.36	2.11	2.87	2.29	3.28	4.15	3.53	4.70	5.83	4.47	5.72	7.32
11	1.36	2.08	2.89	2.27	3.27	4.17	3.50	4.70	5.84	4.40	5.72	7.30
12	1.33	2.03	2.84	2.27	3.22	4.12	3.51	4.63	5.76	4.40	5.64	7.21
13	1.36	2.07	2.85	2.31	3.29	4.19	3.55	4.78	5.92	4.46	5.83	7.44
14	1.35	2.07	2.87	2.27	3.26	4.13	3.52	4.70	5.80	4.43	5.72	7.32
15	1.21	1.94	2.71	2.14	3.05	3.91	3.27	4.32	5.51	4.00	5.23	6.89
16	1.36	2.09	2.90	2.30	3.29	4.22	3.49	4.73	5.92	4.39	5.77	7.35
17	1.37	2.09	2.86	2.31	3.31	4.20	3.53	4.79	5.93	4.46	5.85	7.46
18	1.42	2.19	2.98	2.34	3.41	4.28	3.46	4.89	6.10	4.36	5.95	7.65
19	1.34	2.03	2.85	2.24	3.19	4.08	3.47	4.56	5.67	4.34	5.55	7.13
20	1.38	2.10	2.85	2.32	3.34	4.23	3.51	4.84	6.00	4.46	5.92	7.54